stereotypical temporal and topological manner (Braak and Braak, 1991; Braak et al., 2003). Furthermore, fetal mesencephalic grafts in the striatum of PD patients eventually develop Lewy bodies, suggesting that pathologic α-synuclein could be transmitted from diseased striatal neurons to grafted neurons (Kordower et al., 2008; Li et al., 2008). Cell-cell transmission of tau- and α-synuclein aggregates has been observed in both cell culture and animal models (Clavaguera et al., 2009; de Calignon et al., 2012; Desplats et al., 2009; Frost et al., 2009; Goedert et al., 2010; Liu et al., 2012; Luk et al., 2009, 2012a, 2012b; Nonaka et al., 2010; Masuda-Suzukake et al., 2013). Therefore, prion-like propagation of aberrant protein aggregates may be involved in the pathogenesis of neurodegenerative diseases.

Here, we show that insoluble TDP-43 aggregates in brains of ALS and FTLD-TDP patients have prion-like properties, including the ability to seed intracellular TDP-43 aggregation, stability against heat and proteinases, and cell-to-cell transmissibility.

RESULTS

Intracellular TDP-43 Is Aggregated in a Seed-Dependent Manner

The C-terminal portion of TDP-43 has sequence similarity to prion (Guo et al., 2011). Therefore, to investigate whether intracellular TDP-43 is aggregated in a self-templating manner, like prion, we first established a cell culture model for seeded aggregation of intracellular TDP-43 using SH-SY5Y and 293T cells (Figures 1 and S1A).

We examined whether TDP-43 forms intracellular aggregates in the presence of insoluble TDP-43 prepared from ALS or FTLD-TDP brains as seeds. We observed filamentous structures that were positive for antiphospho TDP-43 (anti-pS409/410) antibody (10–15 nm in diameter) by electron microscopy analyses of insoluble TDP-43 from brains of patients (Figure 1A). Furthermore, it was recently reported that TDP-43 inclusions in ALS and FTLD-TDP showed thioflavin positivity (Bigio et al., 2013). These results clearly indicate that insoluble TDP-43 from brains, used as seeds, had the properties of amyloid. To distinguish plasmid-derived TDP-43 from insoluble TDP-43 introduced as seeds, we used a plasmid encoding hemagglutinin (HA)-tagged TDP-43. SH-SY5Y cells were transiently transfected with HA-tagged TDP-43 and then transduced with or without N-lauroylsarcosine sodium salt (sarkosyl)-insoluble fraction (Sar-ppt) prepared from the brains of ALS (ALS ppt) or FTLD-TDP (FTLD ppt) patients. Cell lysates were fractionated and immunoblotted with anti-HA and anti-pS409/410 antibodies. In cells transfected with HA-TDP-43 plasmid alone, expressed HA-TDP-43 was detected in all fractions with an antibody against HA, whereas phosphorylated HA-TDP-43 was modestly detected in the insoluble fraction (ppt), indicating that the transiently expressed HA-TDP-43 was slightly aggregated (Figure 1B). In cells treated with ALS ppt (5 μg) alone, several bands were detected in ppt fractions with anti-pS409/410, suggesting that endogenous TDP-43 is aggregated in the presence of seeds. On the other hand, in HA-TDP-43-expressing cells transduced with ALS ppt (5 μg), bands with slower mobility were seen with an antibody against HA, and both phosphorylated full-length HA-TDP-43 and its CTFs were detected with anti-pS409/410. We confirmed that plasmid-derived TDP-43, but not ALS ppt seeds, is mainly aggregated in ppt fractions, because no bands were detected with anti-pS409/410 when ALS ppt (5 μg, used as seeds) alone was loaded on the gel (Figure 1C, rightmost lane). Similarly, full-length HA-TDP-43 and CTFs positive for anti-pS409/410 were produced in cells transfected with both HA-TDP-43 plasmid and FTLD ppt (Figures 1B and S1B). Given that plasmid-derived, nontagged TDP-43 was accumulated intracellularly in the presence of ALS ppt (Figure 1C), we mainly used a plasmid encoding, nontagged TDP-43 in subsequent work.

To test whether insoluble TDP-43 in diseased brain extracts can function as seeds for aggregation, we prepared immunodepleted ALS ppt (Figure 1D) as seeds for intracellular TDP-43 aggregation. Sar-ppt of ALS brain was incubated with a mixture of anti-TDP-43 (polyclonal; Proteintech) and anti-pS409/410 antibodies, followed by addition of protein G-Sepharose. After overnight incubation, the supernatant fraction was analyzed by immunoblotting. As shown in Figure 1D (left panel), the immunoreactivity against anti-pS409/410 found in nontreated ALS ppt was wholly lost after immunodepletion (ID). Then, we introduced immunodepleted ALS ppt (ALS ppt ID) into cells expressing HA-TDP-43, using MultiFectam. As shown in Figure 1D (right panel), the band intensities of phosphorylated full-length HA-TDP-43 and CTFs in the ppt fraction of cells expressing HA-TDP-43 and treated with ALS ppt ID were much weaker than those in the case of cells expressing HA-TDP-43 and treated with nonimmunodepleted ALS ppt. We also tested the specificity of ALS ppt as seeds for aggregation of TDP-43. When recombinant α-synuclein fibrils were introduced into cells transiently expressing α-synuclein, phosphorylated α-synuclein was accumulated in Triton-insoluble fractions (Figure S2A), as previously reported (Nonaka et al., 2010). However, intracellular α-synuclein aggregation was not observed in cells expressing α-synuclein and treated with ALS ppt (Figure S2B). Furthermore, HA-TDP-43 was not aggregated in the presence of α-synuclein fibril seeds (Figure S2C). These results showed that insoluble TDP-43 functions specifically as seeds for intracellular aggregation of TDP-43, but not for aggregation of α-synuclein.

We performed immunocytochemical analyses of cells expressing HA-TDP-43 and treated with or without ALS ppt. No phosphorylated and aggregated TDP-43 was seen in cells expressing HA-TDP-43 only (Figure 1E). A few dot-like structures positive for anti-pS409/410 were found in nontransfected cells treated with ALS ppt. On the other hand, round cytoplasmic inclusions of TDP-43 positive for both anti-pS409/410 and an antibody against Ub were detected in cells expressing HA-TDP-43 and treated with ALS ppt. The percentage of HA-positive cells that were also positive for anti-pS409/410 antibody was calculated to be 11.4% ± 4.3%. Interestingly, the immunoreactivity of an antibody against HA in nuclei of cells with cytoplasmic TDP-43 aggregates was less than that in nuclei of cells expressing HA-TDP-43 without aggregates (Figure 1E, lower left), as seen for pathogenic neurons with cytoplasmic TDP-43 inclusions in ALS and FTLD-TDP brains. Taken together, these results suggest that intracellular TDP-43 was efficiently aggregated in cultured cells in a manner that depended on seeding with insoluble TDP-43 derived from patients' brains.

Cell PRESS
Open ACCESS

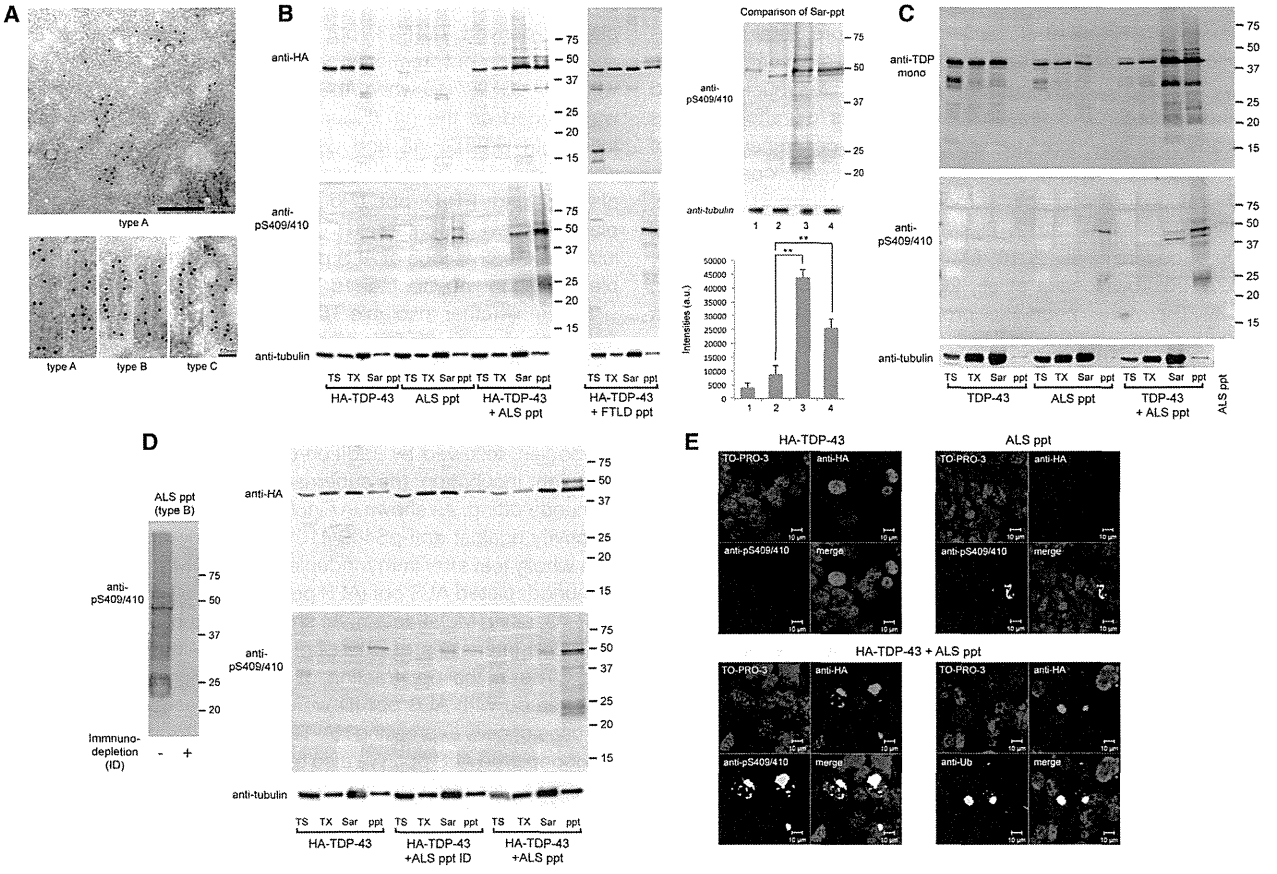

Figure 1. Detergent-Insoluble Fractions from ALS and FTLD-TDP Brains Function as Seeds for Intracellular Aggregation of Plasmid-Derived TDP-43

(A) Immuno-electron microscopy analyses of insoluble fractions from diseased brains (types A, B, and C). Filamentous structures are labeled with anti-phospho TDP-43 antibody (pS409/410). Scale bars represent 200 nm in upper panel, 50 nm in lower panel.

(B) Immunoblot analysis of lysates from cells expressing HA-TDP-43 plasmid only (HA-TDP-43), cells treated with ALS ppt (5 μg; ALS ppt), cells transfected with both HA-TDP-43 and ALS ppt (HA-TDP-43 + ALS ppt), and cells transfected with both HA-TDP-43 and FTLD ppt (5 μg; HA-TDP-43 + FTLD ppt). Proteins were differentially extracted from cells with Tris-HCl (TS), Triton X-100 (TX), and sarkosyl (Sar), leaving the pellet (ppt). Blots were probed using anti-HA (upper) and anti-pS409/410 (lower). In the right panel, the Sar-ppt fractions are shown side by side. 1: HA-TDP-43; 2: ALS ppt; 3: HA-TDP-43 + ALS ppt; 4: HA-TDP-43 + FTLD ppt. The immunoreactivity of each lane that was positive for anti-pS409/410 was quantified and the results are expressed as means + SEM (n = 3). **$p < 0.0005$ by Student's t test; a.u., arbitrary unit.

See also Figure S1.

(C) Immunoblot analysis of proteins extracted from cells expressing only nontagged TDP-43 plasmid (TDP-43), cells treated only with ALS ppt (ALS ppt), and cells transfected with both TDP-43 and ALS ppt (TDP-43 + ALS ppt). Blots were probed using anti-TDP-43 monoclonal antibody (upper) and anti-pS409/410 (lower). No bands were detected when only ALS ppt (5 μg) used as seeds was loaded on the gel (rightmost lane).

(D) ID of ALS ppt was performed with (+) or without (−) a mixture of anti-TDP-43 and anti-pS409/410 antibody. This was followed by immunoblot analyses with anti-pS409/410 (left panel). Proteins differentially extracted from cells expressing only HA-TDP-43 plasmid (HA-TDP-43), and cells transfected with both HA-TDP-43 and immunodepleted ALS ppt (HA-TDP-43 + ALS ppt ID) or untreated ALS ppt (HA-TDP-43 + ALS ppt) were analyzed. Blots were probed using anti-HA (upper) and anti-pS409/410 (lower).

(E) Confocal laser microscopy analyses of cells expressing only HA-TDP-43 plasmid (HA-TDP-43), cells treated with detergent-insoluble fraction of ALS brain (ALS ppt), and cells transfected with both HA-TDP-43 and ALS ppt (HA-TDP-43 + ALS ppt) immunostained with anti-HA (red), anti-pS409/410 (green) or anti-Ub (green), and counterstained with TO-PRO-3 (blue). Scale bars represent 10 μm.

Aggregation of Full-Length TDP-43 Precedes Generation of TDP-43 CTFs

To further investigate the seed-dependent intracellular aggregation of TDP-43, we performed time-course experiments and immunoblot analyses during TDP-43 aggregate formation. Cells expressing HA-TDP-43 and treated with or without ALS ppt were incubated for 1–3 days, and each day the cell lysates were fractionated as described above. No band positive for anti-pS409/410 was detected in any fraction on day 1 or day 2, whereas a weak band of phosphorylated HA-TDP-43 was seen in the insoluble fraction (ppt) on day 3 of cells expressing HA-TDP-43 (Figure 2A). When cells were transfected with both HA-TDP-43

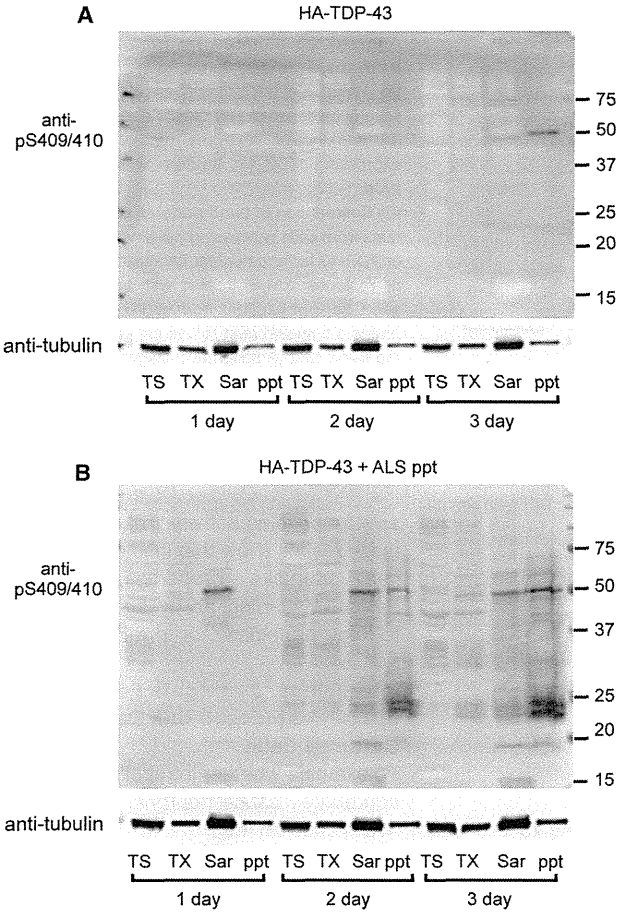

Figure 2. Time Course of Production of TDP-43 CTFs
(A and B) Cells transiently expressing HA-TDP-43 plasmid treated without (A) or with (B) ALS ppt were incubated for 1–3 days and then harvested. Proteins were differentially extracted and subjected to immunoblot analyses. Blots were probed with anti-pS409/410.

plasmid and ALS ppt, surprisingly, full-length HA-TDP-43 was accumulated even on day 1, whereas CTFs were not detected in any fraction at this time (Figure 2B). On and after day 2, not only full-length HA-TDP-43 but also CTFs were aggregated in cells. Thus, intracellular aggregation of full-length TDP-43 precedes generation of TDP-43 CTFs, suggesting that production of CTFs is not essential for formation of intracellular TDP-43 aggregates.

Characteristic CTFs of Insoluble TDP-43 in Each Disease Type Were Reproduced in a Self-Templating Manner in Cultured Cells

TDP-43 proteinopathy is classified into four types based on the predominant TDP-43-positive structures: type A mainly includes FTLD-TDP with GRN mutations, type B contains ALS and FTLD-MND, type C is representative of sporadic FTLD-TDP showing impairment of semantic memory, and type D refers to the pathology associated with inclusion body myopathy with early-onset Paget's disease and frontotemporal dementia caused by *VCP* mutations (Mackenzie et al., 2011). Each type is also characterized biochemically by the patterns of insoluble TDP-43 CTFs detected with anti-pS409/410 (Hasegawa et al., 2008; Tsuji et al., 2012). We prepared Sar-ppt from several types of brains (Figure 3A) and introduced them as seeds into cells expressing a plasmid encoding TDP-43. After 3 days of incubation, cells were harvested and each Sar-ppt was analyzed by immunoblotting with anti-pS409/410. In Figures 3A and 3B, all seeds prepared from TDP-43 proteinopathy brains (Nos. 1–8), but not from DLB (No. 9) or Pick's disease (No. 10) brain, were shown to function as seeds for TDP-43 aggregation in cultured cells, but the seeding efficiencies were different: type A and B seeds were more effective than type C. No sample was available from FTLD-TDP type D brain.

Next, to check whether each characteristic deposit of CTF was reproduced in cultured cells in the presence of each type of seed, we prepared insoluble fractions from TDP-43-expressing cells treated with seeds from each type of brain, and analyzed them by immunoblotting using anti-pS409/410. Interestingly, the band patterns of CTFs in the insoluble fraction (ppt) of cells expressing TDP-43 in the presence of each type of seed were different from each other, but quite similar to that of insoluble TDP-43 prepared as seeds from the corresponding patients (type A, B, or C), indicating that plasmid-derived TDP-43 is aggregated in a template-dependent manner in the presence of each type of seed (Figure 3C). These results suggest that seed-dependent TDP-43 aggregation, like prion aggregation, occurs in a self-templating manner. Insoluble TDP-43 from diseased brains appears to have features similar to those of pathogenic prion.

Insoluble TDP-43 Has Prion-like Properties

Next, we examined whether insoluble TDP-43 from brains of patients has prion-like characteristics. First, we tested whether detergent-insoluble TDP-43 prepared from cells containing TDP-43 aggregates as well as seeds from brains can promote intracellular TDP-43 aggregation. Triton X-100 (TX)-insoluble fraction was prepared as seeds from cells containing aggregates (Figure 4A, right panel) and introduced into cells. In a control experiment, we confirmed that insoluble seeds from cells expressing HA-TDP-43 treated with ALS ppt (HA-TDP-43+ALS ppt) did not serve efficiently as seeds for endogenous TDP-43 aggregation (Figure S3A). In cells expressing HA-TDP-43 and treated with TX-insoluble seeds from cells transfected with both HA-TDP-43 and ALS ppt, phosphorylated full-length HA-TDP-43 and CTFs were observed in the insoluble fraction (ppt; Figure 4A), whereas the band of phosphorylated full-length HA-TDP was hardly detectable in the insoluble fraction from cells expressing HA-TDP-43 and treated with TX-insoluble seed from cells without transfection (none) or treated with TX-insoluble seed from cells expressing HA-TDP-43 alone (HA-TDP-43). In immunocytochemical analyses of cells expressing HA-TDP-43 and treated with TX-insoluble seeds from cells transfected with both HA-TDP-43 and ALS ppt (HA-TDP-43+ALS ppt), we observed inclusions positive for both anti-pS409/410 and anti-Ub (Figure 4B), which were very similar to those observed in cells expressing

Cell PRESS
Open ACCESS

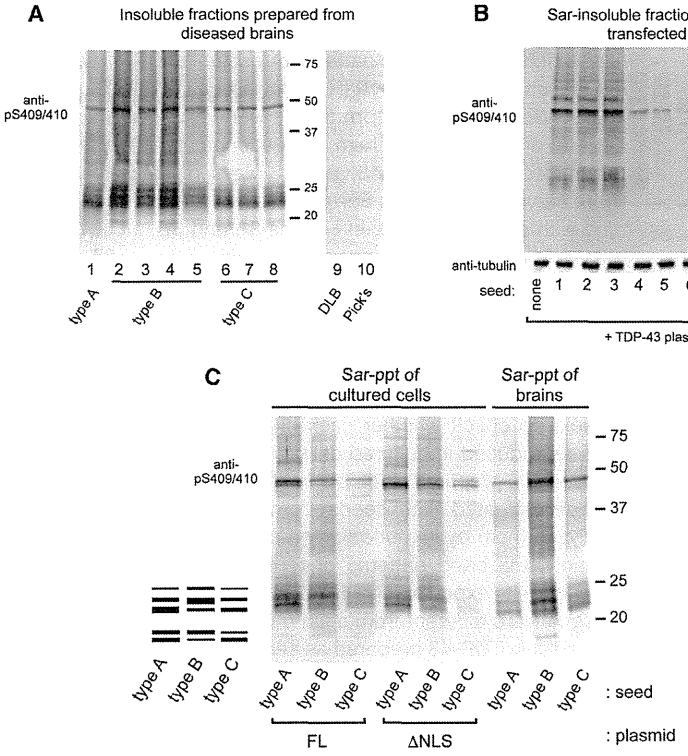

Figure 3. Formation of Self-Templating Aggregates Induced by Insoluble TDP-43 from the Brains of Patients

(A) Immunoblot analyses of Sar-ppt prepared from several diseased brains used as seeds.

(B) Immunoblot analyses of Sar-ppt of cells expressing TDP-43 treated with each seed (Nos. 1–10).

(C) Comparison of band patterns of Sar-ppt fractions from cells expressing full-length TDP-43 (FL) or TDP-43 lacking nuclear localization signal (78–84 residues: ΔNLS) treated with type A, B, or C seed. Sar-ppt fractions from each of the diseased brains are shown next to cellular ppt fractions on the same blot. A schematic diagram of the band pattern of TDP-43 CTFs is also presented. Blots were probed using anti-pS409/410.

HA-TDP-43 treated with ALS ppt (Figure 1E). These results indicate that TX-insoluble seeds produced from cells containing TDP-43 aggregates can function as seeds for further aggregation of TDP-43.

We also checked the effects of heat treatment or proteinase digestion of insoluble TDP-43 on seeding ability. Each type of seed was treated or not treated at 100°C for 5 min (boiling) and analyzed by immunoblotting with anti-pS409/410. No marked differences in the band patterns of each type of seed were seen before or after the boiling treatment (Figure 4C, left panel). Then, these seeds were introduced into TDP-43-expressing cells, and Sar-ppts prepared from the cells were analyzed by immunoblotting with anti-pS409/410 (Figures 4C and S3B). In the case of type A seed, the seeding effect on TDP-43 aggregation was unaffected by boiling, whereas the ability of type B and C seeds to induce TDP-43 aggregation was almost abrogated after boiling (Figure 4C, middle and right panels). All of these seeds were easily degraded into <20 kDa CTFs by Proteinase K (ProK) treatment (Figure 4D, left panel). However, seeding ability to induce intracellular TDP-43 aggregation was retained even after ProK digestion (Figure 4D, middle and right panels, and Figure S3C).

Furthermore, we tested whether formic acid, which destroys the β-sheet structure of proteins, influences the seeding ability of insoluble TDP-43. As shown in Figures 4E, S3D, and S3E, insoluble fractions from type A, B, and C brains treated with formic acid did not induce intracellular TDP-43 aggregation, suggesting that β-sheet-rich structure is necessary for seeding activity. Taken together, these results show that insoluble TDP-43 has prion-like properties, including repeated seeding ability and sensitivity to heat, proteinase, or formic acid.

Intracellular Aggregate Formation of TDP-43 Induces Cell Death in Cultured Cells

To examine whether intracellular TDP-43 aggregates cause neuronal dysfunction leading to cell death, we measured the rate of cell death in cells containing intracellular TDP-43 aggregates by means of lactate dehydrogenase (LDH) assay. Cells transfected with TDP-43 were treated with insoluble fractions from TDP-43 proteinopathy brains or Pick's disease brain and incubated for 3 days, followed by LDH assay. As shown in Figure 5A, the rate of cell death was almost 5% in cells treated only with insoluble fractions from type B or plasmid transfection, whereas it was ~20% in cells expressing TDP-43 and treated with each TDP-43 proteinopathy brain extract. These cell lysates were also analyzed by immunoblotting. Increased cell death of these cells was accompanied by deposition of phosphorylated TDP-43 in the Sar-ppt fraction (Figure 5B). However, no significant cell death was observed in cells expressing TDP-43 and treated with Pick's disease brain extract, in which phosphorylated TDP-43 was not deposited. These results suggest that increased cell death of cells containing TDP-43 aggregates is correlated with the amount of intracellular TDP-43 aggregates.

Intracellular Accumulation of TDP-43 Aggregates Elicits Proteasome Dysfunction

Previously, we reported that proteasome activity was suppressed in cells containing intracellular α-synuclein aggregates (Nonaka et al., 2010). To examine whether intracellular aggregates of TDP-43 also induce proteasome dysfunction, we assayed proteasome activity in cells containing TDP-43 aggregates by using the GFP-CL1 reporter (Bence et al., 2001), which is available to monitor proteasome activity in cultured cells (Nonaka and Hasegawa, 2009; Nonaka et al., 2010).

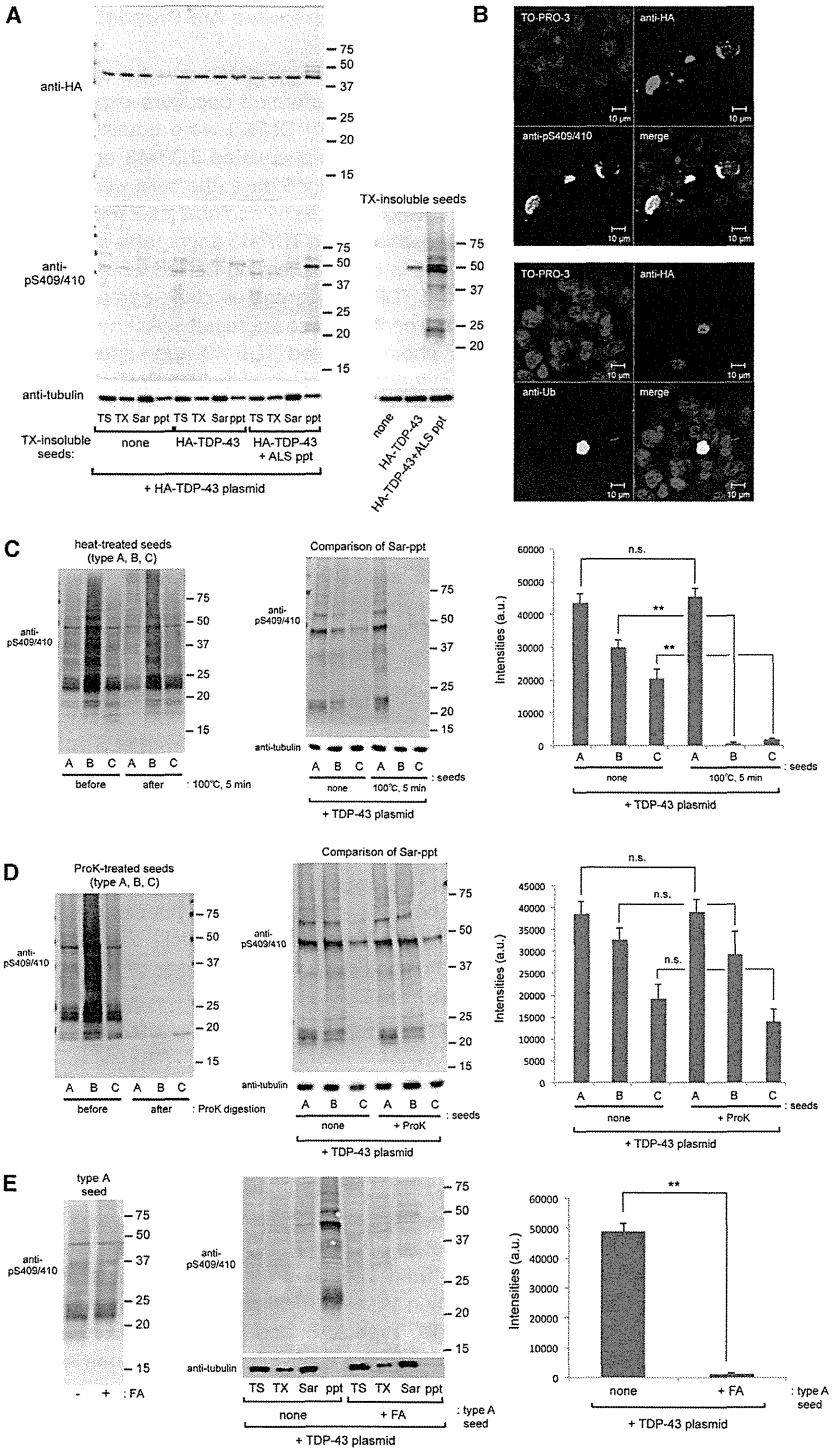

Figure 4. Characterization of the Prion-like Properties of Detergent-Insoluble TDP-43 from Brains

(A) Immunoblot analyses of cells expressing HA-TDP-43 and treated with Triton X-100-insoluble fractions (TX-insoluble seeds) prepared from the following cells, using anti-HA (upper) and anti-pS409/410 (lower): none, mock cells; HA-TDP-43, cells expressing HA-TDP-43; and HA-TDP-43+ALS ppt, cells expressing HA-TDP-43 and treated with ALS ppt. These TX-insoluble seeds (10 μg each) were also immunoblotted with anti-pS409/410 (lower right).

(B) Confocal laser microscopy analyses of cells expressing HA-TDP-43 and treated with TX-insoluble seed from cells transfected with both HA-TDP-43 and ALS ppt (HA-TDP-43+ALS ppt) immunostained with anti-HA (red), anti-pS409/410 (green), or anti-Ub (green), and counterstained with TO-PRO-3 (blue). Scale bars: 10 μm.

(C) Effect of heat treatment on the seeding ability of each type of seed. Each seed before and after heat treatment (100°C for 5 min) was analyzed by immunoblotting using anti-pS409/410 (left). Then, cells expressing TDP-43 were treated with these fractions as seeds. After 3 days of incubation, Sar-ppt fractions were prepared and analyzed by immunoblotting using anti-pS409/410 (middle). The immunoreactivity of each lane that was positive for anti-pS409/410 was quantified and the results are expressed as means + SEM (n = 3). **p < 0.0001 by Student's t test; n.s., not significant; a.u., arbitrary unit. See also Figure S3.

(D) Effect of ProK on the seeding ability of each type of seed. Each seed before and after ProK digestion (final 20 μg/mL ProK at 37°C for 30 min) was analyzed by immunoblotting using anti-pS409/410 (left). Then, cells expressing TDP-43 were treated with these fractions as seeds. After 3 days of incubation, the Sar-ppt fractions were analyzed by immunoblotting using anti-pS409/410 (middle). The immunoreactivity of each lane that was positive for anti-pS409/410 was quantified and the results are expressed as means + SEM (n = 3). n.s., not significant; a.u., arbitrary unit. See also Figure S3.

(E) Effect of formic acid (FA) on the seeding ability of type A seed. Type A seed with or without FA treatment was analyzed by immunoblotting using anti-pS409/410 (left). Then, cells expressing TDP-43 were treated with these fractions as seeds. After 3 days of incubation, fractionated samples were analyzed by immunoblotting using anti-pS409/410 (right). The immunoreactivity of ppt fractions that were positive for anti-pS409/410 was quantified and the results are expressed as means + SEM (n = 3). **p < 0.0001 by Student's t test. a.u., arbitrary unit. See also Figure S3.

Cells were transfected with TDP-43 and GFP-CL1 plasmids overnight, followed by transduction of ALS ppt. After 3 days of incubation, the cells were analyzed by confocal microscopy and immunoblotting. As shown in Figures 6A and 6B, GFP fluorescence in cells transfected with GFP-CL1 alone was very low due to degradation of GFP-CL1 by proteasome. When cells expressing GFP-CL1 were treated with proteasome inhibitor MG132 (0.1 μM), GFP fluorescence intensity

Cell PRESS
Open ACCESS

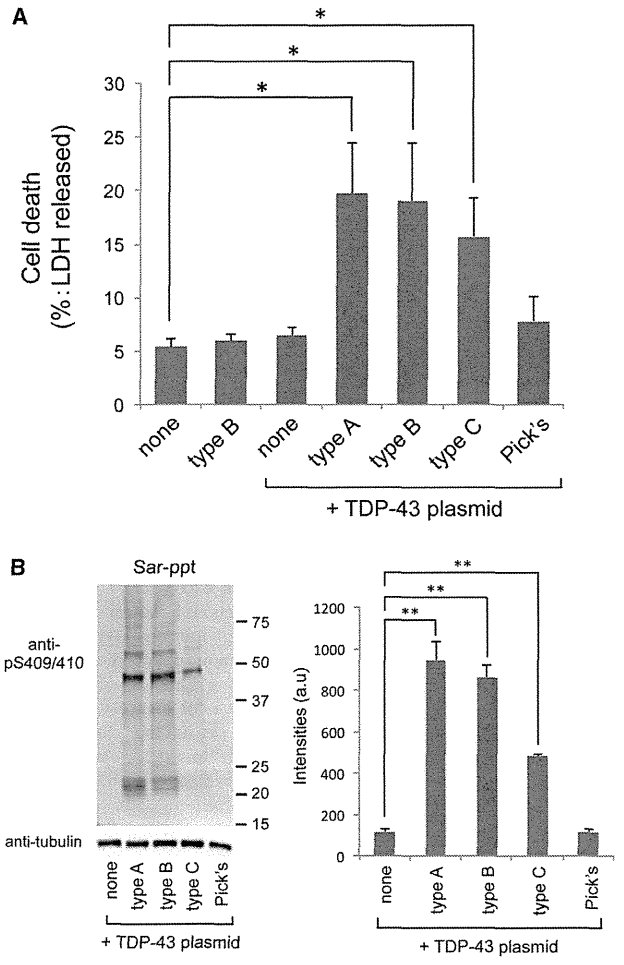

Figure 5. Cell Death Induced by the Formation of Intracellular TDP-43 Aggregates

(A) The extent of cell death of transfected cells was quantified by an LDH release assay. Cells treated with type B seed alone (type B), cells transfected with TDP-43 plasmid alone, or cells expressing TDP-43 and treated with Sar-ppt from type A, B, or C, or Pick's disease brains were cultured, and a cell death assay was performed 3 days thereafter. The results are expressed as means + SEM (n = 5). *$p < 0.05$ versus "none" by Student's t test.

(B) Immunoblot analyses of Sar-ppt from cells expressing TDP-43 and treated with extracts of type A, B, C, and Pick's disease brains, using anti-pS409/410. Immunoreactivity to anti-pS409/410 was quantified in each lane. The results are expressed as means + SEM (n = 3). **$p < 0.001$ versus "none" by Student's t test. a.u., arbitrary unit.

was significantly higher. GFP fluorescence in cells transfected with TDP-43 alone or treated with ALS ppt alone was as low as that in cells expressing only GFP-CL1, whereas it was significantly higher in cells expressing TDP-43 and treated with ALS ppt. We confirmed that cells containing phosphorylated TDP-43 aggregates were strongly positive for GFP (Figure 6C). These results suggest that proteasome activity is suppressed in cells harboring intracellular TDP-43 aggregates.

Phosphorylated TDP-43 Aggregates Are Propagated between Cultured Cells

To examine whether TDP-43 aggregates can be transferred between cultured cells, we performed coculture experiments. SH-SY5Y cells expressing only DsRed were cocultured with SH-S5Y5 cells harboring phosphorylated TDP-43 aggregates in a 1:1 ratio. After incubation for 3 days, the cells were stained with anti-pS409/410 and analyzed by confocal laser microscopy. The presence of phosphorylated TDP-43 aggregates immunolabeled with Alexa-488 in cells expressing DsRed would indicate that phosphorylated TDP-43 aggregates could spread to cells that originally did not contain these aggregates. As shown in Figures 7A and 7B, phosphorylated TDP-43 aggregates (green) were found in the cytoplasm of cells expressing DsRed. The percentage of DsRed-positive cells that also contained phosphorylated TDP-43 aggregates was calculated to be 2.9% ± 0.8%. In three-dimensional image modeling of a DsRed-expressing cell with TDP-43 aggregates, the signal of phosphorylated TDP-43 aggregates was merged with that of DsRed in the X-Z and Y-Z cross-sections (Figure 7B).

Next, we examined how TDP-43 aggregates are released from cells. It has been hypothesized that protein aggregates are released via exosome (Fevrier et al., 2004; Goedert et al., 2010). To investigate whether this mechanism operates for TDP-43 aggregates, we prepared exosome fractions from cells expressing TDP-43 plasmid alone, cells treated with ALS ppt alone, or cells expressing TDP-43 and treated with ALS ppt using the ExoQuick-TC kit (SBI). Immunoblot analyses showed that in cells expressing TDP-43 and treated with ALS ppt, the band intensity of full-length TDP-43 in the exosome fraction was significantly increased as compared with that in cells transfected with TDP-43 plasmid or ALS ppt alone (Figure 7C), whereas expression of the exosome marker protein CD63 was similar in all of the exosome fractions. These results suggest the possibility that exosome may contribute to the release of intracellular TDP-43 aggregates.

DISCUSSION

Prion-like propagation of aggregated proteins in neurodegenerative diseases is well established (Clavaguera et al., 2009; Desplats et al., 2009; Frost et al., 2009; Goedert et al., 2010; Kordower et al., 2008; Li et al., 2008; Luk et al., 2009; Nonaka et al., 2010; Masuda-Suzukake et al., 2013; Polymenidou and Cleveland, 2011; Ren et al., 2009). Here, we show that insoluble TDP-43 prepared from TDP-43 proteinopathy brains (type A, B, and C) can function as seeds for intracellular TDP-43 aggregation in cultured cells. Type A, B, and C brains showed distinct banding patterns of TDP-43 CTFs in immunoblot analyses with anti-pS409/410 (Hasegawa et al., 2008; Tsuji et al., 2012). The band patterns of characteristic CTFs are thought to reflect structural differences of TDP-43 fibrils deposited in each type of brain (Hasegawa et al., 2008; Tsuji et al., 2012). Interestingly, band patterns of CTFs characteristic of the individual seeds were seen in intracellular TDP-43 aggregates in cultured cells, indicating that plasmid-derived TDP-43 aggregation occurs in a self-templating manner. The seeding activity of insoluble TDP-43 from patients' brains was stable against detergents, heat

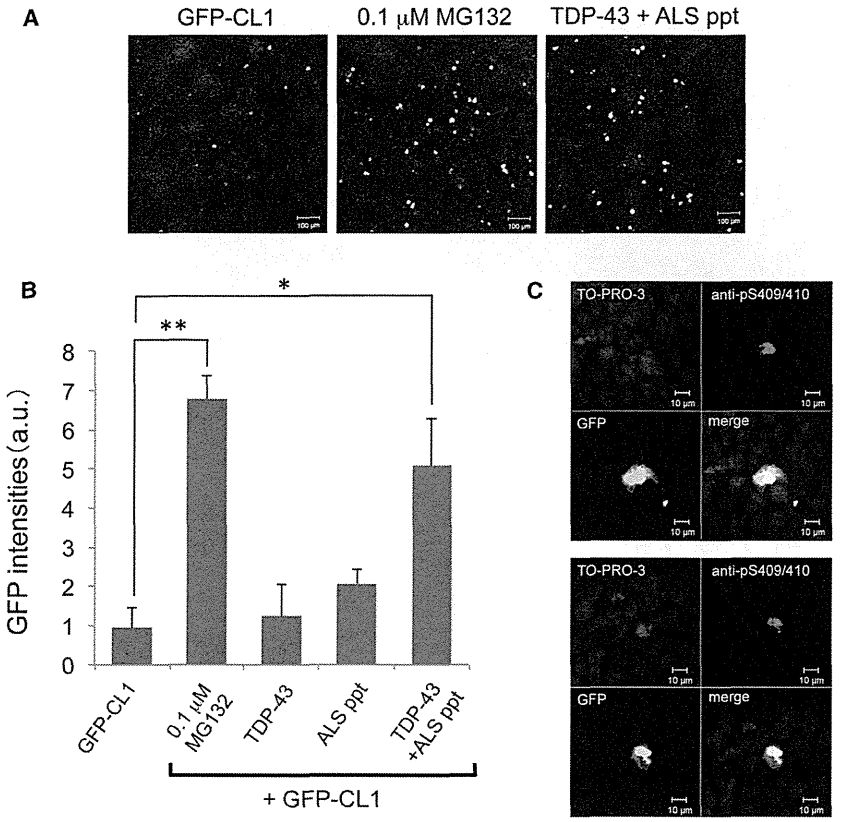

Figure 6. Proteasome Dysfunction in Cells Bearing Intracellular TDP-43 Aggregates

(A–C) SH-SY5Y cells transfected with both GFP-CL1 and TDP-43 were treated with ALS ppt for 2 days.

(A) As a control, cells expressing GFP-CL1 with or without 0.1 μM MG132 or ALS ppt, and cells expressing both GFP-CL1 and TDP-43 were also analyzed.

(B) The intensity of GFP fluorescence in these cells was quantified. The results are expressed as means + SEM (n = 3). *$p < 0.05$; **$p < 0.001$ versus the value of GFP-CL1 by Student's t test. a.u., arbitrary unit.

(C) Cells transfected with both GFP-CL1 and TDP-43 and treated with ALS ppt were stained with anti-pS409/410.

treatment, or proteolytic digestion, and cell-to-cell transmission ability was retained. Formic acid abrogated the seeding ability, suggesting that β-sheet structure in insoluble TDP-43 is indispensable for this ability. Thus, insoluble TDP-43 in the brains of patients has the characteristics of a pathogenic prion, suggesting that TDP-43 proteinopathy involves mechanisms similar to those of prion disease. It remains unclear, however, how protein aggregates spread between cells in vivo. It seems likely that prion-like aggregates are released from cells and taken up by neighboring cells, where they penetrate the cytoplasm and act as nuclei for further aggregation (Goedert et al., 2010). Prions are transferred between cultured cells via exosomes or tunneling nanotubes (Fevrier et al., 2004; Gousset et al., 2009), and our results indicate that TDP-43 aggregates may also be transferred from cell to cell at least partly via exosomes. Further investigation is needed to elucidate in detail the mechanisms of intercellular propagation of protein aggregates in vitro and in vivo. Nevertheless, taken together, our data suggest that TDP-43 proteinopathy can be classified as a prion disease.

Phosphorylated TDP-43 CTFs, as well as phosphorylated full-length TDP-43, are deposited in affected neurons in TDP-43 proteinopathy (Hasegawa et al., 2008, 2011). TDP-43 CTFs identified in FTLD-TDP brains are more prone to form aggregates than the full-length molecule in cultured cells (Igaz et al., 2009; Nonaka et al., 2009). Further, they bind with full-length TDP-43 and may facilitate aggregation of full-length TDP-43 in cultured cells (Budini et al., 2012; Nonaka et al., 2009; Zhang et al., 2009). Therefore, generation of pathogenic TDP-43 CTFs may be crucial for the formation of intracellular TDP-43 inclusions leading to neuronal cell death. However, our time-course immunoblotting analyses (Figure 2) showed that full-length TDP-43 aggregation preceded the deposition of CTFs, suggesting that cleavage of TDP-43 to produce CTFs is not a trigger for intracellular TDP-43 aggregate formation. Thus, it appears that the generation of CTFs is a consequence of degradation of phosphorylated full-length TDP-43 to eliminate abnormal and toxic aggregates of TDP-43, rather than a cause of aggregation of full-length TDP-43. In other words, TDP-43 CTFs deposited in affected neurons represent the residual stable core portion of TDP-43 aggregates left after degradation by intracellular proteolytic systems.

Abnormal posttranslational modifications and abnormal structure of seeds for aggregation are important for reproducing the pathological and biochemical features of TDP-43 inclusions found in the brains of patients with TDP-43 proteinopathy in cultured cells. Indeed, intracellular TDP-43 aggregates obtained using recombinant TDP-43 fibrils as seeds appeared as very small dot-like structures without phosphorylation (Furukawa et al., 2011), and were quite different from the TDP-43 inclusions found in the brains of patients. Our model for seeded aggregation of TDP-43 seems consistent with the pathological and biochemical changes found in the brains of patients with TDP-43 proteinopathy: in the model, aggregated TDP-43 is phosphorylated and ubiquitinated, and immunoreactivity of TDP-43 in nuclei of cells containing cytoplasmic TDP-43 aggregates is relatively weak. We also observed significant cell death and proteasome dysfunction associated with the presence of intracellular TDP-43 aggregates. It is possible that such proteasome dysfunction is caused by overloading of the ubiquitin-proteasome system with ubiquitinated proteins, including TDP-43 aggregates. The resulting suppression of proteasome activity might induce cell death. We previously observed a similar phenomenon (Nonaka et al., 2010); i.e., seed-dependent intracellular

Cell PRESS
Open ACCESS

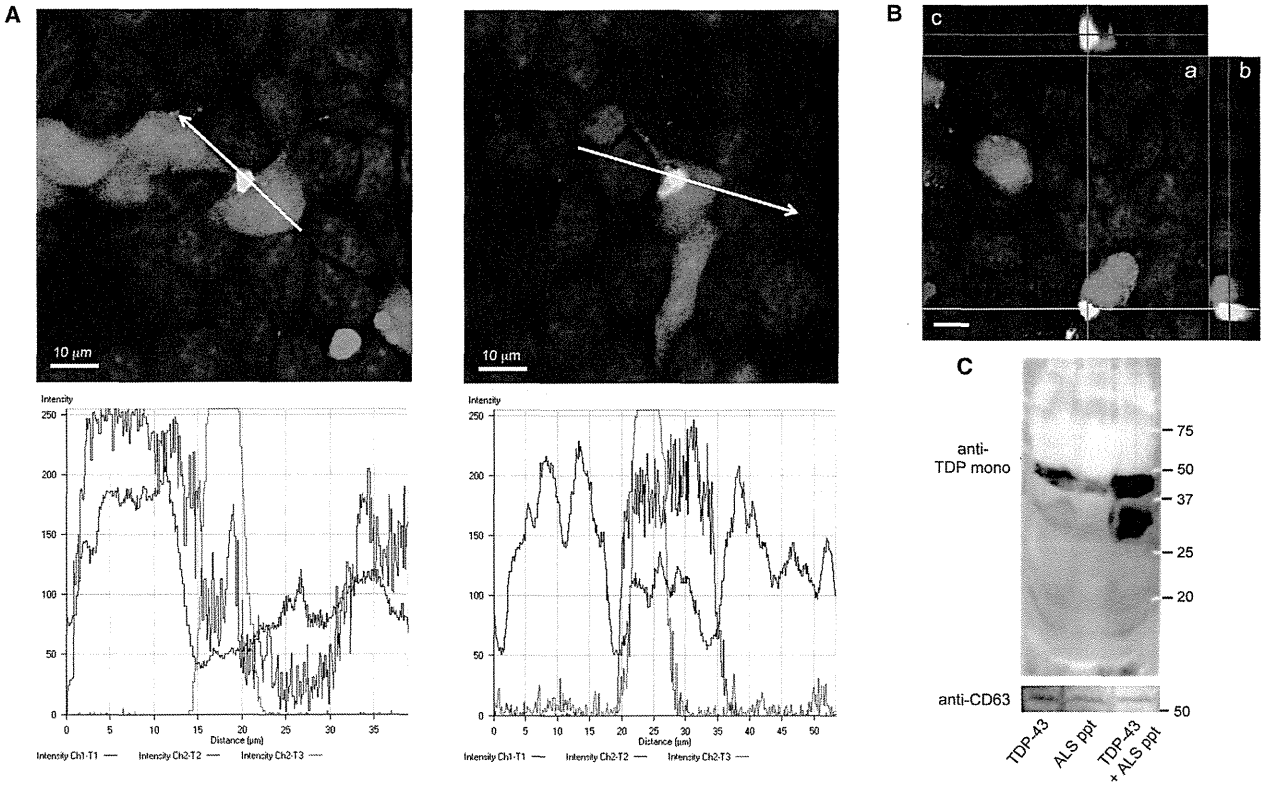

Figure 7. Intracellular TDP-43 Aggregates Are Released in Association with Exosome

(A) Coculture of cells expressing DsRed and cells having intracellular TDP-43 aggregates in a 1:1 ratio. After incubation for 3 days, cells were stained with pS409/410 (green) and counterstained with TO-PRO-3 (blue). The graphs show the intensity distribution profile of DsRed (red line), phosphorylated TDP-43 (green line), and TO-PRO-3, a nuclear marker (blue line), in the merged image. Scale bars: 10 μm.

(B) Cross-sections of reconstructed TDP-43 aggregates in these cocultured cells. (a) One of the optical sections (X-Y) at the depth indicated with blue lines in (b) and (c). (b) Cross-sectional Y-Z image along the green line indicated in (a). (c) Cross-sectional X-Z image along the red line indicated in (a). Red, DsRed; green, phosphorylated TDP-43 aggregate positive for anti-pS409/410; blue, TO-PRO-3 (nuclei). Scale bars: 10 μm.

(C) Immunoblot analyses of exosome fractions prepared from culture medium of cells expressing TDP-43 (TDP-43), cells treated with ALS ppt alone (ALS ppt), and cells expressing TDP-43 and treated with ALS ppt (TDP-43+ALS ppt). Blots were probed with anti-TDP-43 monoclonal (ProteinTech) and an antibody against CD63 (SBI).

aggregation of α-synuclein caused proteasome dysfunction and cell death.

In summary, our results show that insoluble TDP-43 in the brains of patients has prion-like features, and we consider that the onset and progression of TDP-43 proteinopathy may be associated with the propagation of TDP-43 aggregates between neuronal cells. If this is so, suppressing the propagation of aggregated proteins may be a new therapeutic strategy for many neurodegenerative diseases.

EXPERIMENTAL PROCEDURES

Preparation of Detergent-Insoluble Fractions from Brains of Patients

Human brain tissues were obtained from Fukushimura Hospital, Aichi Medical University (Aichi, Japan), Shizuoka Institute of Epilepsy and Neurological Disorders (Shizuoka, Japan), and Tokyo Metropolitan Institute of Gerontology (Tokyo, Japan). This study was approved by the local research ethics committee of Tokyo Metropolitan Institute of Medical Science (approval No. 12-3). The subjects included four patients with ALS, one with FTLD-TDP type A, three with FTLD-TDP type C, one with dementia with Lewy bodies, and one with Pick's disease. All patients with ALS met the revised El Escorial criteria for ALS (Brooks, 1994) without dementia. All patients with FTLD-TDP met the clinical diagnostic criteria of FTLD (Neary et al., 1998), and TDP-43 subtypes were classified according to published guidelines (Mackenzie et al., 2011).

Brain samples (0.5 g) from patients with ALS, FTLD-TDP, or Pick's disease were each homogenized in 2.5 ml of homogenization buffer (HB: 10 mM Tris-HCl, pH 7.5 containing 0.8 M NaCl, 1 mM EGTA, 1 mM dithiothreitol). Sarkosyl was added to the lysates (final concentration: 1%), which were then incubated for 30 min at 37°C, and centrifuged at 12,000 *g* for 10 min at room temperature. The supernatant was further centrifuged at 100,000 *g* for 10 min at room temperature. The pellet was suspended in 2 ml PBS by sonication. Lysates were divided into four tubes (each 500 μL) and centrifuged at 100,000 *g* for 20 min at room temperature. The resulting pellets were used as the detergent-insoluble fraction (ppt).

For immuno-electron microscopy analyses, the detergent-insoluble fractions prepared from brains were placed on collodion-coated, 300-mesh copper grids and stained with anti-pS409/410 and 2% (v/v) phosphotungstate. Micrographs were recorded on a JEOL JEM-1400 electron microscope.

In ID experiments, mixtures of anti-pS409/410 and anti-TDP-43 polyclonal antibody (Proteintech; 2 μl each) were added to 20 μl of ALS ppt suspension

in PBS, followed by addition of 10 μl of protein G-Sepharose (Sigma). After overnight incubation at 4°C, the supernatant was recovered. As a control, the other half of the lysate was incubated with a mixture of nonspecific mouse and rabbit immunoglobulin G (IgG; Cosmo Bio) and the same amount of protein G-Sepharose. An 8 μl aliquot of the supernatant was introduced into cells as described below.

In formic acid treatment, the detergent-insoluble fractions were suspended in 100 μl of 100% (v/v) formic acid (Nacalai Tesque) and incubated at room temperature for 30 min. After incubation, 900 μl of water was added and the mixtures were evaporated. The resulting residues were suspended in 500 μl of 0.1 M triethylammonium bicarbonate buffer (Fluka) and evaporated again. The residues were also suspended in 500 μl of water and centrifuged at 100,000 *g* for 20 min at room temperature. The resulting pellets were suspended in 100 μl of PBS and the mixtures were used for introduction experiments (see below).

Cell Culture and Transfection of Expression Plasmids

Human neuroblastoma SH-SY5Y cells obtained from ATCC were cultured in Dulbecco's modified Eagle's medium (DMEM)/F12 medium (Sigma-Aldrich) supplemented with 10% (v/v) fetal calf serum, penicillin-streptomycin-glutamine (Gibco), and MEM nonessential amino acids solution (Gibco). The cells were maintained at 37°C under a humidified atmosphere of 5% (v/v) CO_2 in air. They were grown to 50% confluence in six-well culture dishes for transient expression and then transfected with expression plasmids (usually 1 μg) using FuGENE6 (Roche) according to the manufacturer's instructions. Under our conditions, the efficiency of transfection using pEGFP-C1 vector was 20%–30%.

Introduction of Insoluble Proteins into Cells

Detergent-insoluble fractions prepared as described above were suspended in 150 μl PBS by sonication. Then 5 μg of insoluble fraction was mixed with 120 μl of Opti-MEM (Gibco), and 62.5 μl of Multifectam was added. After incubation for 30 min at room temperature, 62.5 μl of Opti-MEM was added and incubation was continued for 5 min at room temperature. Then, the mixtures were added to cells (mock cells or cells expressing HA-TDP-43, non-tagged TDP-43, or TDP-43 ΔNLS) and incubation was continued for 6 hr in a CO_2 incubator. After incubation, the medium was changed to fresh DMEM/F12 and culture was continued for the indicated period in each case. The cells were harvested and cellular proteins were differentially extracted and immunoblotted with the indicated antibodies, as previously described (Nonaka et al., 2010). Under our conditions, the efficiency of introduction of brain extracts was ~10%.

Confocal Microscopy

SH-SY5Y cells on coverslips were transfected with the indicated plasmids and cultured for 14 hr as described above. Then, the detergent-insoluble fraction was introduced and culture was continued for ~1–2 days. After fixation with 4% paraformaldehyde, cells were stained with the appropriate primary and secondary antibodies as described previously (Nonaka et al., 2010). Fluorescence was analyzed with a laser scanning confocal fluorescence microscope (LSM5 Pascal; Carl Zeiss). Confocal Z slices with an interval of 0.2 or 0.5 μm were obtained and reconstructed for three-dimensional observation using LSM5 Pascal v 4.0 software.

Cell Death Assay

Cell death assays were performed using a CytoTox 96 Non-Radioactive Cytotoxicity Assay Kit (Promega).

Assay of Proteasome Activity

In a GFP-reporter assay to monitor proteasome activity in cultured cells by confocal laser microscopy, SH-SY5Y cells that had been transfected with pcDNA3-HA-TDP-43 (1 μg) and GFP-CL1 (0.3 μg) using FuGENE6 and then treated with detergent-insoluble fraction of ALS brain were grown on coverslips for 2 days or treated with 0.1 μM MG132 overnight (Nonaka and Hasegawa, 2009; Nonaka et al., 2010). These cells were analyzed with the use of a laser-scanning confocal fluorescence microscope (LSM5Pascal; Carl Zeiss).

Coculture of Cells

SH-SY5Y cells transiently expressing DsRed (3 days after transfection) were mixed equally with cells expressing TDP-43 and treated with ALS ppt (3 days after introduction of ALS ppt). The cocultured cells were grown for a further 3 days, fixed with 4% paraformaldehyde, stained with anti-pS409/410 and TO-PRO-3, and observed under a laser-scanning confocal fluorescence microscope (LSM5Pascal; Carl Zeiss).

Preparation of Exosome Fractions

Exosome fractions were prepared from 4 ml of culture medium of cells expressing TDP-43, cells treated with ALS ppt, or cells transfected with both TDP-43 and ALS ppt, which had been cultured for 3 days after transfection, using an ExoQuick-TC kit from SBI according to the manufacturer's protocol. The exosome fractions were dissolved in 100 μl of SDS sample buffer and immunoblotted.

Statistical Analysis

Statistical analyses were performed using GraphPad Prism 4 software (GraphPad Software). Biochemical data were statistically analyzed using the unpaired, two-tailed Student's t test. A p value of ≤ 0.05 was considered to be statistically significant. For further details regarding the materials and methods used in this work, see Extended Experimental Procedures.

SUPPLEMENTAL INFORMATION

Supplemental Information includes Extended Experimental Procedures and three figures and can be found with this article online at http://dx.doi.org/10.1016/j.celrep.2013.06.007.

ACKNOWLEDGMENTS

We thank Makiko Yamashita and Masato Hosokawa for helpful comments. This work was supported by a Grant-in-Aid for Scientific Research (C) (JSPS KAKENHI 22500345 to T.N.), a Grant-in-Aid for Scientific Research (S) (JSPS KAKENHI 23228004 to M.H.) a Grant-in-Aid for Scientific Research (A) (JSPS KAKENHI 23240050 to M.H.), MHLW Grant (Number 12946221 to M.H.), a Grant-in-Aid for Scientific Research on Innovative Area "Brain Environment" (MEXT KAKENHI 24111556 to T.N.), and a grant from the Takeda Science Foundation (to T.N.).

Received: March 12, 2013
Revised: May 17, 2013
Accepted: June 6, 2013
Published: July 3, 2013

REFERENCES

Arai, T., Hasegawa, M., Akiyama, H., Ikeda, K., Nonaka, T., Mori, H., Mann, D., Tsuchiya, K., Yoshida, M., Hashizume, Y., and Oda, T. (2006). TDP-43 is a component of ubiquitin-positive tau-negative inclusions in frontotemporal lobar degeneration and amyotrophic lateral sclerosis. Biochem. Biophys. Res. Commun. *351*, 602–611.

Arai, T., Hasegawa, M., Nonoka, T., Kametani, F., Yamashita, M., Hosokawa, M., Niizato, K., Tsuchiya, K., Kobayashi, Z., Ikeda, K., et al. (2010). Phosphorylated and cleaved TDP-43 in ALS, FTLD and other neurodegenerative disorders and in cellular models of TDP-43 proteinopathy. Neuropathology *30*, 170–181.

Bence, N.F., Sampat, R.M., and Kopito, R.R. (2001). Impairment of the ubiquitin-proteasome system by protein aggregation. Science *292*, 1552–1555.

Bigio, E.H., Wu, J.Y., Deng, H.X., Bit-Ivan, E.N., Mao, Q., Ganti, R., Peterson, M., Siddique, N., Geula, C., Siddique, T., and Mesulam, M. (2013). Inclusions in frontotemporal lobar degeneration with TDP-43 proteinopathy (FTLD-TDP) and amyotrophic lateral sclerosis (ALS), but not FTLD with FUS proteinopathy (FTLD-FUS), have properties of amyloid. Acta Neuropathol. *125*, 463–465.

Braak, H., and Braak, E. (1991). Neuropathological stageing of Alzheimer-related changes. Acta Neuropathol. *82*, 239–259.

Braak, H., Del Tredici, K., Rüb, U., de Vos, R.A., Jansen Steur, E.N., and Braak, E. (2003). Staging of brain pathology related to sporadic Parkinson's disease. Neurobiol. Aging *24*, 197–211.

Brooks, B.R. (1994). El Escorial World Federation of Neurology criteria for the diagnosis of amyotrophic lateral sclerosis. Subcommittee on Motor Neuron Diseases/Amyotrophic Lateral Sclerosis of the World Federation of Neurology Research Group on Neuromuscular Diseases and the El Escorial "Clinical Limits of Amyotrophic Lateral Sclerosis" workshop contributors. J. Neurol. Sci. *124(Suppl)*, 96–107.

Budini, M., Buratti, E., Stuani, C., Guarnaccia, C., Romano, V., De Conti, L., and Baralle, F.E. (2012). Cellular model of TAR DNA binding protein 43 (TDP-43) aggregation based on its C-terminal Q/N rich region. J. Biol. Chem. *287*, 7512–7525.

Buratti, E., and Baralle, F.E. (2009). The molecular links between TDP-43 dysfunction and neurodegeneration. Adv. Genet. *66*, 1–34.

Buratti, E., Dörk, T., Zuccato, E., Pagani, F., Romano, M., and Baralle, F.E. (2001). Nuclear factor TDP-43 and SR proteins promote in vitro and in vivo CFTR exon 9 skipping. EMBO J. *20*, 1774–1784.

Clavaguera, F., Bolmont, T., Crowther, R.A., Abramowski, D., Frank, S., Probst, A., Fraser, G., Stalder, A.K., Beibel, M., Staufenbiel, M., et al. (2009). Transmission and spreading of tauopathy in transgenic mouse brain. Nat. Cell Biol. *11*, 909–913.

de Calignon, A., Polydoro, M., Suárez-Calvet, M., William, C., Adamowicz, D.H., Kopeikina, K.J., Pitstick, R., Sahara, N., Ashe, K.H., Carlson, G.A., et al. (2012). Propagation of tau pathology in a model of early Alzheimer's disease. Neuron *73*, 685–697.

Desplats, P., Lee, H.J., Bae, E.J., Patrick, C., Rockenstein, E., Crews, L., Spencer, B., Masliah, E., and Lee, S.J. (2009). Inclusion formation and neuronal cell death through neuron-to-neuron transmission of alpha-synuclein. Proc. Natl. Acad. Sci. USA *106*, 13010–13015.

Fevrier, B., Vilette, D., Archer, F., Loew, D., Faigle, W., Vidal, M., Laude, H., and Raposo, G. (2004). Cells release prions in association with exosomes. Proc. Natl. Acad. Sci. USA *101*, 9683–9688.

Frost, B., Jacks, R.L., and Diamond, M.I. (2009). Propagation of tau misfolding from the outside to the inside of a cell. J. Biol. Chem. *284*, 12845–12852.

Furukawa, Y., Kaneko, K., Watanabe, S., Yamanaka, K., and Nukina, N. (2011). A seeding reaction recapitulates intracellular formation of Sarkosyl-insoluble transactivation response element (TAR) DNA-binding protein-43 inclusions. J. Biol. Chem. *286*, 18664–18672.

Goedert, M., Clavaguera, F., and Tolnay, M. (2010). The propagation of prion-like protein inclusions in neurodegenerative diseases. Trends Neurosci. *33*, 317–325.

Gousset, K., Schiff, E., Langevin, C., Marijanovic, Z., Caputo, A., Browman, D.T., Chenouard, N., de Chaumont, F., Martino, A., Enninga, J., et al. (2009). Prions hijack tunnelling nanotubes for intercellular spread. Nat. Cell Biol. *11*, 328–336.

Guo, W., Chen, Y., Zhou, X., Kar, A., Ray, P., Chen, X., Rao, E.J., Yang, M., Ye, H., Zhu, L., et al. (2011). An ALS-associated mutation affecting TDP-43 enhances protein aggregation, fibril formation and neurotoxicity. Nat. Struct. Mol. Biol. *18*, 822–830.

Hasegawa, M., Arai, T., Nonaka, T., Kametani, F., Yoshida, M., Hashizume, Y., Beach, T.G., Buratti, E., Baralle, F., Morita, M., et al. (2008). Phosphorylated TDP-43 in frontotemporal lobar degeneration and amyotrophic lateral sclerosis. Ann. Neurol. *64*, 60–70.

Hasegawa, M., Nonaka, T., Tsuji, H., Tamaoka, A., Yamashita, M., Kametani, F., Yoshida, M., Arai, T., and Akiyama, H. (2011). Molecular dissection of TDP-43 proteinopathies. J. Mol. Neurosci. *45*, 480–485.

Igaz, L.M., Kwong, L.K., Chen-Plotkin, A., Winton, M.J., Unger, T.L., Xu, Y., Neumann, M., Trojanowski, J.Q., and Lee, V.M. (2009). Expression of TDP-43 C-terminal fragments in vitro recapitulates pathological features of TDP-43 proteinopathies. J. Biol. Chem. *284*, 8516–8524.

Kordower, J.H., Chu, Y., Hauser, R.A., Freeman, T.B., and Olanow, C.W. (2008). Lewy body-like pathology in long-term embryonic nigral transplants in Parkinson's disease. Nat. Med. *14*, 504–506.

Li, J.Y., Englund, E., Holton, J.L., Soulet, D., Hagell, P., Lees, A.J., Lashley, T., Quinn, N.P., Rehncrona, S., Björklund, A., et al. (2008). Lewy bodies in grafted neurons in subjects with Parkinson's disease suggest host-to-graft disease propagation. Nat. Med. *14*, 501–503.

Liu, L., Drouet, V., Wu, J.W., Witter, M.P., Small, S.A., Clelland, C., and Duff, K. (2012). Trans-synaptic spread of tau pathology in vivo. PLoS ONE *7*, e31302.

Luk, K.C., Song, C., O'Brien, P., Stieber, A., Branch, J.R., Brunden, K.R., Trojanowski, J.Q., and Lee, V.M. (2009). Exogenous alpha-synuclein fibrils seed the formation of Lewy body-like intracellular inclusions in cultured cells. Proc. Natl. Acad. Sci. USA *106*, 20051–20056.

Luk, K.C., Kehm, V., Carroll, J., Zhang, B., O'Brien, P., Trojanowski, J.Q., and Lee, V.M. (2012a). Pathological α-synuclein transmission initiates Parkinson-like neurodegeneration in nontransgenic mice. Science *338*, 949–953.

Luk, K.C., Kehm, V.M., Zhang, B., O'Brien, P., Trojanowski, J.Q., and Lee, V.M. (2012b). Intracerebral inoculation of pathological α-synuclein initiates a rapidly progressive neurodegenerative α-synucleinopathy in mice. J. Exp. Med. *209*, 975–986.

Mackenzie, I.R., Neumann, M., Baborie, A., Sampathu, D.M., Du Plessis, D., Jaros, E., Perry, R.H., Trojanowski, J.Q., Mann, D.M., and Lee, V.M. (2011). A harmonized classification system for FTLD-TDP pathology. Acta Neuropathol. *122*, 111–113.

Masuda-Suzukake, M., Nonaka, T., Hosokawa, M., Oikawa, T., Arai, T., Akiyama, H., Mann, D.M.A., and Hasegawa, M. (2013). Prion-like spreading of pathological α-synuclein in brain. Brain *136*, 1128–1138.

Neary, D., Snowden, J.S., Gustafson, L., Passant, U., Stuss, D., Black, S., Freedman, M., Kertesz, A., Robert, P.H., Albert, M., et al. (1998). Frontotemporal lobar degeneration: a consensus on clinical diagnostic criteria. Neurology *51*, 1546–1554.

Neumann, M., Sampathu, D.M., Kwong, L.K., Truax, A.C., Micsenyi, M.C., Chou, T.T., Bruce, J., Schuck, T., Grossman, M., Clark, C.M., et al. (2006). Ubiquitinated TDP-43 in frontotemporal lobar degeneration and amyotrophic lateral sclerosis. Science *314*, 130–133.

Nonaka, T., and Hasegawa, M. (2009). A cellular model to monitor proteasome dysfunction by alpha-synuclein. Biochemistry *48*, 8014–8022.

Nonaka, T., Kametani, F., Arai, T., Akiyama, H., and Hasegawa, M. (2009). Truncation and pathogenic mutations facilitate the formation of intracellular aggregates of TDP-43. Hum. Mol. Genet. *18*, 3353–3364.

Nonaka, T., Watanabe, S.T., Iwatsubo, T., and Hasegawa, M. (2010). Seeded aggregation and toxicity of alpha-synuclein and tau: cellular models of neurodegenerative diseases. J. Biol. Chem. *285*, 34885–34898.

Pesiridis, G.S., Lee, V.M., and Trojanowski, J.Q. (2009). Mutations in TDP-43 link glycine-rich domain functions to amyotrophic lateral sclerosis. Hum. Mol. Genet. *18*(R2), R156–R162.

Polymenidou, M., and Cleveland, D.W. (2011). The seeds of neurodegeneration: prion-like spreading in ALS. Cell *147*, 498–508.

Ren, P.H., Lauckner, J.E., Kachirskaia, I., Heuser, J.E., Melki, R., and Kopito, R.R. (2009). Cytoplasmic penetration and persistent infection of mammalian cells by polyglutamine aggregates. Nat. Cell Biol. *11*, 219–225.

Sephton, C.F., Good, S.K., Atkin, S., Dewey, C.M., Mayer, P., 3rd, Herz, J., and Yu, G. (2010). TDP-43 is a developmentally regulated protein essential for early embryonic development. J. Biol. Chem. *285*, 6826–6834.

Snowden, J.S., Neary, D., and Mann, D.M. (2002). Frontotemporal dementia. Br. J. Psychiatry *180*, 140–143.

Tsuji, H., Arai, T., Kametani, F., Nonaka, T., Yamashita, M., Suzukake, M., Hosokawa, M., Yoshida, M., Hatsuta, H., Takao, M., et al. (2012). Molecular analysis and biochemical classification of TDP-43 proteinopathy. Brain *135*, 3380–3391.

Wu, L.S., Cheng, W.C., Hou, S.C., Yan, Y.T., Jiang, S.T., and Shen, C.K. (2010). TDP-43, a neuro-pathosignature factor, is essential for early mouse embryogenesis. Genesis *48*, 56–62.

Zhang, Y.J., Xu, Y.F., Cook, C., Gendron, T.F., Roettges, P., Link, C.D., Lin, W.L., Tong, J., Castanedes-Casey, M., Ash, P., et al. (2009). Aberrant cleavage of TDP-43 enhances aggregation and cellular toxicity. Proc. Natl. Acad. Sci. USA *106*, 7607–7612.

Neurobiology of Aging 34 (2013) 1101–1104

Contents lists available at SciVerse ScienceDirect

Neurobiology of Aging

journal homepage: www.elsevier.com/locate/neuaging

Brief communication

Suspected limited efficacy of γ-secretase modulators

Nobuto Kakuda [a,b], Kohei Akazawa [c], Hiroyuki Hatsuta [d], Shigeo Murayama [d], Yasuo Ihara [a,b,e,f,*], The Japanese Alzheimer's Disease Neuroimaging Initiative

[a] Department of Neuropathology, Faculty of Life and Medical Sciences, Doshisha University, Kyoto, Japan
[b] Core Research for Evolutional Science and Technology (CREST), Japan Science and Technology Agency, Saitama, Japan
[c] Department of Medical Informatics, Niigata University Medical and Dental Hospital, Niigata University, Niigata, Japan
[d] Department of Neuropathology, Tokyo Metropolitan Institute of Gerontology, Tokyo, Japan
[e] Center for Neurologic Diseases, Doshisha University, Kyoto, Japan
[f] New Energy and Industrial Technology Development Organization (NEDO), Kanagawa, Japan

ARTICLE INFO

Article history:
Received 16 June 2012
Accepted 25 August 2012
Available online 9 October 2012

Keywords:
γ-Secretase
γ-Modulator
Alzheimer's disease

ABSTRACT

Mild cognitive impairment and Alzheimer's disease (AD) are associated with changes in γ-secretase activity in the brain, producing an amyloid β-protein-42-lowering γ-modulator-like effect. We show here that this modulation occurs at the stage of amyloid deposition, presumably decades earlier than the onset of AD. In addition, γ-secretase modulator-1, a γ-modulator, altered γ-secretase activity in the AD brain but to a lesser extent than in the normal brain. These findings suggest that γ-modulators have limited efficacy against amyloid deposition and AD.

1. Introduction

Amyloid β-protein (Aβ) is cleaved sequentially from amyloid precursor protein by β- and γ-secretases (for a review see Selkoe, 2001). The longer but minor species, Aβ42, predominates in senile plaques (Iwatsubo et al., 1994). γ-Secretase, a heterogeneous complex (Takasugi et al., 2003; Serneels et al., 2009), governs the intramembrane proteolysis of type I membrane proteins including amyloid precursor protein (Sisodia and St George-Hyslop, 2002; Wakabayashi and De Strooper, 2008). We found recently that γ-secretase activity is altered in brains affected by mild cognitive impairment (MCI) or Alzheimer's disease (AD). The change decreases the concentrations of both Aβ42 and Aβ43 in cerebrospinal fluid (CSF) in patients affected with MCI or AD. To compensate for these decreases, the levels of Aβ38 and Aβ40 are increased (Kakuda et al., 2012). We assume that Aβ42 and Aβ43 are enhanced to be converted by stepwise processing to Aβ38 and Aβ40, respectively, by altered γ-secretase in the brain affected by MCI or AD (Kakuda et al., 2012; Takami et al., 2009). Reciprocal changes in the levels of Aβ42 and Aβ38 without a change in the total Aβ level are an essential characteristic of γ-secretase modulators, drugs whose development receives intense attention.

2. Materials and methods

2.1. Subjects

Human cortical specimens for quantification of raft-associated γ-secretase activity were obtained from brains that had been removed, processed, and stored at −80 °C within 12 hours postmortem; the bodies had been placed in a cold (4 °C) room within 2 hours after death. The specimens were kept at the Brain Bank at Tokyo Metropolitan Institute of Gerontology. For all the brains registered at the bank we obtained written informed consent for their use for medical research from the patient or the patient's family. Each brain specimen (approximately 0.5 g) was taken from Brodmann areas 9–11 of 13 AD patients (80 ± 5.0 years of age; Braak neurofibrillary tangle [NFT] stage >IV; senile plaque [SP] stage = C; retrospective clinical dementia rating [CDR] >1), 10 SP stage B patients (76 ± 4.0 years of age; Braak NFT stage >I; retrospective CDR = 0), 10 SP stage A patients (76 ± 4.7 years of age; Braak NFT stage >0; retrospective CDR = 0), and 16 controls in SP stage 0 (77 ± 6.5 years of age; Braak NFT stage <I; retrospective CDR = 0). SP stages were determined by modified methenamine silver stain: stage A: Aβ deposits in the basal portions of the isocortex; stage B: Aβ deposits in virtually all isocortical association

* Corresponding author at: Department of Neuropathology, Faculty of Life and Medical Sciences, Doshisha University, 4-1-1, Kizugawadai, Kizugawa, Kyoto 619-0225, Japan. Tel.: +81 774 65 6058; fax: +81 3 5800 6852.
E-mail address: yihara@mail.doshisha.ac.jp (Y. Ihara).

0197-4580/$ – see front matter © 2013 Elsevier Inc. All rights reserved.
http://dx.doi.org/10.1016/j.neurobiolaging.2012.08.017

areas except primary centers; stage C (AD): Aβ deposits in all areas of the isocortex including primary motor and sensory centers (Braak and Braak, 1991).

2.2. Quantification of brain raft-associated γ-secretase activity

A previously reported assay method was employed with some modifications (Kakuda et al., 2012). Briefly, each raft fraction, adjusted to 100 μg/mL in protein concentration, was incubated with 200 nM of βCTF-FLAG for 1 hour at 37 °C in the presence of 0, or 0.1–0.5 μM γ-secretase modulator (GSM)-1 (kindly provided by Dr M. Okochi, Osaka University). After incubation, all samples were centrifuged at 265,000*g* on a TLA110 rotor (Beckman, Palo Alto, CA, USA) for 20 minutes at 4 °C. The supernatants were separated on sodium dodecyl sulfate polyacylamide gel electrophoresis (SDS-PAGE), and subjected to quantitative Western blot analysis, using specific antibodies, 3B1 for Aβ38, BA27 for Aβ40, 44A3 for Aβ42, and anti-Aβ43 polyclonal for Aβ43.

2.3. GSM-1-induced shift of ln(Aβ38/42)

Shifts of ln(Aβ38/42) with GSM-1 were calculated as GSM-1-induced ln(Aβ38/42) minus the ratio measured in its absence.

2.4. Statistical analysis

All statistical analyses were performed using SPSS version 14.0. Data transformation was required to achieve normal distributions; all analyses were performed after logarithmic transformation of the data for Aβ38, Aβ40, Aβ42, and Aβ43. Analysis of variance was used to test the equality of mean values for continuous variables between the 4 groups: control, SP stage A, SP stage B, and AD. Multiple comparisons were made using Bonferroni *t* test to test the differences between controls, SP stage A, SP stage B, and AD. The paired *t* test was used to examine the effect of GSM-1 treatment. *p* values <0.05 were considered significant.

3. Results

We speculated that this modulation in the γ-secretase activity occurs much earlier than the onset of AD because lower Aβ42 concentrations in CSF appear to be associated with amyloid deposition itself (Fagan et al., 2006). To confirm this, we measured the activities of raft-associated γ-secretase prepared from autopsied brains using a previously established method (Kakuda et al., 2012). Raft fractions were prepared from control and AD brains (Brodmann areas 9–11), which were judged histochemically to be in the Braak SP stage 0, stage A, stage B, or stage C (AD) (Braak and Braak, 1991). Aβs produced by γ-secretase from each brain specimen were analyzed by quantitative Western blot, and the ln(Aβ40/43) and ln(Aβ38/42) ratios were obtained. Stage A plots nearly superimposed with control plots (Fig. 1; 0 vs. A: $p = 1.000$ for ln(Aβ40/43), $p = 1.000$ for ln(Aβ38/42)). However, the γ-secretase activities differed between stage B specimens and 0/A specimens (0 vs. B: $p = 0.005$ for ln(Aβ40/43) and $p < 0.001$ for ln(Aβ38/42); A vs. B: $p = 0.002$ for ln(Aβ40/43) and $p = 0.001$ for ln(Aβ38/42); Fig. 1). AD (stage C) plots were shifted the most (0 vs. C: $p < 0.001$ for ln(Aβ40/43) and $p = 0.003$ for ln(Aβ38/42); A vs. C: $p < 0.001$ for ln(Aβ40/43) and $p = 0.007$ for ln(Aβ38/42)). Most interestingly, although AD plots were shifted to the same extent as stage B plots for Aβ38/42 (B vs. C: $p = 1.000$ for ln(Aβ38/42)), stage B and AD plots differ for Aβ40/43 (B vs. C: $p < 0.001$ for ln(Aβ40/43); Fig. 1).

Although these data were obtained from a cross-sectional study, one might assume that stage A develops through to stage B and eventually to stage C over decades (Duyckaerts and Hauw, 1997).

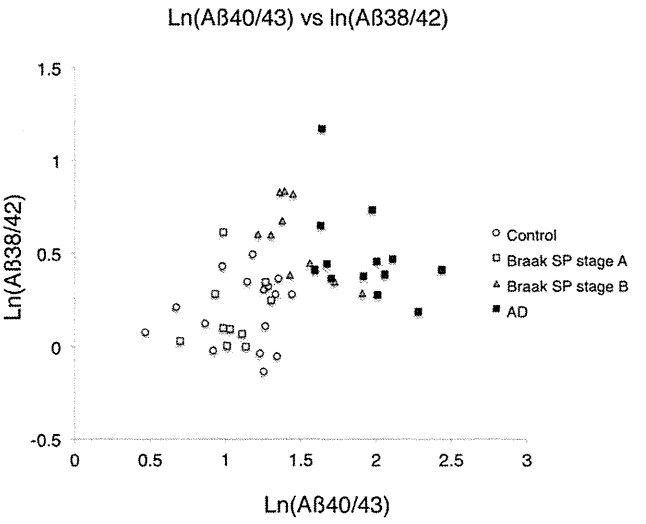

Fig. 1. Ln(amyloid-β protein [Aβ]40/43) versus ln(Aβ38/42) plot of raft-associated γ-secretase prepared from the brains in various (Braak) senile plaque (SP) stages. The raft-associated γ-secretase prepared from Braak SP stages 0, A, B, and C (AD) brain specimens were incubated with 200 nM of βCTF for 1 hour at 37 °C. After centrifugation of the reaction mixtures, the supernatants were saved for quantitative Western blot analysis of Aβs using specific antibodies.

Thus, the Aβ42 product line of γ-secretase appears to undergo changes early and the Aβ42-lowering activity remains constant through to development of AD. By contrast, the Aβ40 product line gradually changes with increasing Aβ40/43 ratio, as stage 0/A develops to stage B and finally to AD. Our previous observations showed that Aβ42 levels in CSF parallel the Aβ38/42 ratio, and Aβ43 levels parallel the Aβ40/43 ratio (Kakuda et al., 2012). These findings suggest that a decrease in the Aβ42 level would be the first alteration observable in CSF and that the level does not change throughout the disease course, whereas the Aβ43 level in CSF would decrease progressively up to AD.

We noted previously that the effects of Aβ42-lowering γ-modulators could be minimal in sporadic MCI/AD patients because modulation of γ-secretase has already begun in their brains. As mentioned above, the modulation of γ-secretase is evident in stage B. Accordingly, we investigated the response of γ-secretase to GSM-1, an Aβ42-lowering modulator, in control and AD brains. We reasoned that a strong response of the altered γ-secretase to GSM-1 would indicate that the drug might still be effective.

We quantified γ-secretase activities in the absence or presence of GSM-1 in control and AD specimens. This agent is known to aggressively modulate only conversion from Aβ42 to Aβ38, but not that from Aβ43 to Aβ40 (Crump et al., 2011; Ebke et al., 2011; Ohki et al., 2011). As expected, GSM-1 treatment significantly lowered Aβ42 and increased Aβ38 in control (see Supplementary Fig. 1). By contrast, in AD specimens, GSM-1 lowered Aβ42 and increased Aβ38 but to a lesser extent (Supplementary Fig. 1). The generation of Aβ40 and Aβ43, and the total production of Aβ were unchanged by the treatment of GSM-1 in all specimens (Supplementary Fig. 1).

In AD specimens, conversion of Aβ43 to Aβ40 seems to be altered compared with control (Kakuda et al., 2012), but this might be due to high concentrations of GSM-1 (>0.5 μM), which suppressed Aβ40 (and Aβ43) product line and total Aβ production in both control and AD specimens (data not shown). GSM-1 treatment significantly elevated the ratio of Aβ38/42 in control (Aβ38/42 with dimethyl sulfoxide vs. Aβ38/42 with GSM-1; $p < 0.000$, paired *t* test; Fig. 2A). By contrast, the same treatment of AD specimens

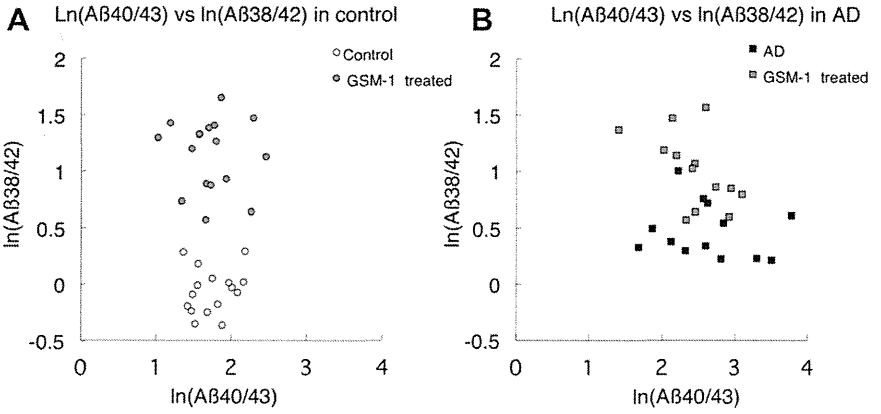

Fig. 2. Ln(amyloid-β protein [Aβ]40/43) versus ln(Aβ38/42) plot of γ-secretase modulator (GSM)-1-treated raft-associated γ-secretase activity. The raft-associated γ-secretases prepared from control (A) and AD (B) brains were incubated with 200 nM of βCTF for 1 hour at 37 °C in the presence of dimethyl sulfoxide or 0.3 μM GSM-1. Aβs produced were quantified by quantitative Western blot analysis using specific antibodies.

caused a much smaller increase in the Aβ38/42 ratio ($p < 0.001$ for AD paired t test; Fig. 2B). There was no significant difference in the Aβ40/43 ratio between control and AD specimens (Aβ40/43 with dimethyl sulfoxide vs. Aβ40/43 with GSM-1; $p = 0.814$ for control; $p = 0.223$ for AD, respectively; paired t test; Fig. 2A and B). The modulating effect on the Aβ38/42 ratio can be interpreted as indicating the extent of GSM-1-induced shift in the Aβ38/42 ratio (Supplementary Table 1). γ-Secretase was associated with significantly lower ratios in AD specimens than in control specimens (control vs. AD: $p < 0.001$), indicating a poor response to GSM-1 in AD specimens.

4. Discussion

Modulation of γ-secretase occurs in AD brains (Kakuda et al., 2012), and to a significant extent already at the stage of amyloid deposition, a decade or even decades before the onset of AD (Duyckaerts and Hauw, 1997). Although γ-secretase self-modulates and produces less Aβ42, it is likely that β-amyloid accumulation slowly progresses and ultimately extends throughout the brain, finally involving primary cortical centers (Duyckaerts and Hauw, 1997). A gradual decline in the rate of Aβ accumulation curve (Kawarabayashi et al., 2001) might be caused by self-modulation of γ-secretase. Currently, we do not know which comes first, Aβ deposition or γ-self-modulation. However, the efficacy of GSM-1 and γ-modulators in general would be limited when Aβ42 deposition and self-modulation of γ-secretase begins in the brain. To date, the efficacy of γ-modulators has been confirmed most often using younger Tg2576 mice, which do not yet accumulate Aβ (Borgegard et al., 2012; Kounnas et al., 2010). In Tg2576 mice, Aβ deposition starts at 9–12 months, and γ-secretase activity changes together with increasing Aβ deposition in the brain starting at 15–16 months of age (Kawarabayashi et al., 2001; data not shown). Thus, the true effectiveness of γ-modulators in Tg2576 mice should be assessed after 15–16 months of age. It is unclear whether γ-modulators are effective in such amyloid-bearing aged mice.

Disclosure statement

The authors have no conflict of interest.

Ethic permission was approved by Faculty of Life and Medical Sciences, Doshisha University, and we obtained written informed consent for their use for medical research from the patient or the patient's family.

Acknowledgements

The authors thank Dr Masayasu Okochi, Neuropsychiatry and Neurochemistry, Department of Integrated Medicine, Osaka University Graduate School of Medicine, for kindly providing GSM-1, and Dr Satoru Funamoto, Department of Neuropathology, Faculty of Life and Medical Sciences, Doshisha University, for providing βCTF. This project was supported in part by the New Energy and Industrial Technology Development Organization, Japan (J-ADNI) and by the MEXT-Supported Program for the Strategic Research Foundation at Private Universities, 2012–2017.

Appendix A. Supplementary data

Supplementary data associated with this article can be found, in the online version, at http://dx.doi.org/10.1016/j.neurobiolaging.2012.08.017.

References

Borgegard, T., Juréus, A., Olsson, F., Rosqvist, S., Sabirsh, A., Rotticci, D., Paulsen, K., Klintenberg, R., Yan, H., Waldman, M., Stromberg, K., Nord, J., Johansson, J., Regner, A., Parpal, S., Malinowsky, D., Radesater, A.C., Li, T., Singh, R., Eriksson, H., Lundkvist, J., 2012. First and second generation γ-secretase modulators (GSMs) modulate amyloid-β (Aβ) peptide production through different mechanisms. J. Biol. Chem. 287, 11810–11819.

Braak, H., Braak, E., 1991. Neuropathological stageing of Alzheimer-related changes. Acta Neuropathol. 82, 239–259.

Crump, C.J., Fish, B.A., Castro, S.V., Chau, D.M., Gertsik, N., Ahn, K., Stiff, C., Pozdnyakov, N., Bales, K.R., Johnson, D.S., Li, Y.M., 2011. Piperidine acetic acid based γ-secretase modulators directly bind to Presenilin-1. ACS Chem. Neurosci. 2, 705–710.

Duyckaerts, C., Hauw, J.J., 1997. Prevalence, incidence and duration of Braak's stages in the general population: can we know? Neurobiol. Aging 18, 362–369.

Ebke, A., Luebbers, T., Fukumori, A., Shirotani, K., Haass, C., Baumann, K., Steiner, H., 2011. Novel γ-secretase enzyme modulators directly target presenilin protein. J. Biol. Chem. 286, 37181–37186.

Fagan, A.M., Mintun, M.A., Mach, R.H., Lee, S.Y., Dence, C.S., Shah, A.R., LaRossa, G.N., Spinner, M.L., Klunk, W.E., Mathis, C.A., DeKosky, S.T., Morris, J.C., Holtzman, D.M., 2006. Inverse relation between in vivo amyloid imaging load and cerebrospinal fluid Abeta42 in humans. Ann. Neurol. 59, 512–519.

Iwatsubo, T., Odaka, A., Suzuki, N., Mizusawa, H., Nukina, N., Ihara, Y., 1994. Visualization of Aβ42(43) and Aβ40 in senile plaque with end-specific Aβ monoclonals: evidence that an initially deposited forms is Aβ42(43). Neuron 13, 45–53.

Kakuda, N., Shoji, M., Arai, H., Furukawa, K., Ikeuchi, T., Akazawa, K., Takami, M., Hatsuta, H., Murayama, S., Hashimoto, Y., Miyajima, M., Arai, H., Nagashima, Y., Yamaguchi, H., Kuwano, R., Nagaike, K., Ihara, Y., Japanese Alzheimer's Disease Neuroimaging Initiative, 2012. Altered γ-secretase activity in mild cognitive impairment and Alzheimer's disease. EMBO Mol. Med. 4, 344–352.

Kawarabayashi, T., Younkin, L.H., Saido, T.C., Shoji, M., Ashe, K.H., Younkin, S.G., 2001. Age-dependent changes in brain, CSF, and plasma amyloid (β) protein in the Tg2576 transgenic mouse model of Alzheimer's disease. J. Neurosci. 21, 372–381.

Kounnas, M.Z., Danks, A.M., Cheng, S., Tyree, C., Ackerman, E., Zhang, X., Ahn, K., Nguyen, P., Comer, D., Mao, L., Yu, C., Pleynet, D., Digregorio, P.J., Velicelebi, G., Stauderman, K.A., Comer, W.T., Mobley, W.C., Li, Y.M., Sisodia, S.S., Tanzi, R.E., Wagner, S.L., 2010. Modulation of gamma-secretase reduces beta-amyloid deposition in a transgenic mouse model of Alzheimer's disease. Neuron 67, 769–780.

Ohki, Y., Higo, T., Uemura, K., Shimada, N., Osawa, S., Berezovska, O., Yokoshima, S., Fukuyama, T., Tomita, T., Iwatsubo, T., 2011. Phenylpiperidine-type γ-secretase modulators target the transmembrane domain 1 of presenilin 1. EMBO J. 30, 4815–4824.

Selkoe, D.J., 2001. Alzheimer's disease: genes, proteins, and therapy. Physiol. Rev. 81, 741–766.

Serneels, L., Van Biervliet, J., Craessaerts, K., Dejaegere, T., Horré, K., Van Houtvin, T., Esselmann, H., Paul, S., Schäfer, M.K., Berezovska, O., Hyman, B.T., Sprangers, B., Sciot, R., Moons, L., Jucker, M., Yang, Z., May, P.C., Karran, E., Wiltfang, J., D'Hooge, R., De Strooper, B., 2009. γ-Secretase heterogeneity in the Aph1 subunit: relevance for Alzheimer's disease. Science 324, 639–642.

Sisodia, S.S., St George-Hyslop, P.H., 2002. gamma-Secretase, Notch, Abeta and Alzheimer's disease: where do the presenilins fit in? Nat. Rev. Neurosci. 3, 281–290.

Takami, M., Nagashima, Y., Sano, Y., Ishihara, S., Morishima-Kawashima, M., Funamoto, S., Ihara, Y., 2009. γ-Secretase: successive tripeptide and tetrapeptide release from the transmembrane domain of β-carboxyl terminal fragment. J. Neurosci. 29, 13042–13052.

Takasugi, N., Tomita, T., Hayashi, I., Tsuruoka, M., Niimura, M., Takahashi, Y., Thinakaran, G., Iwatsubo, T., 2003. The role of presenilin cofactors in the γ-secretase complex. Nature 422, 438–441.

Wakabayashi, T., De Strooper, B., 2008. Presenilins: members of the gamma-secretase quartets, but part-time soloists too. J. Physiol. 23, 194–204.

BMJ open accessible medical research

Multicentre multiobserver study of diffusion-weighted and fluid-attenuated inversion recovery MRI for the diagnosis of sporadic Creutzfeldt–Jakob disease: a reliability and agreement study

Koji Fujita,[1] Masafumi Harada,[2] Makoto Sasaki,[3] Tatsuhiko Yuasa,[4] Kenji Sakai,[5] Tsuyoshi Hamaguchi,[5] Nobuo Sanjo,[6] Yusei Shiga,[7] Katsuya Satoh,[8] Ryuichiro Atarashi,[8] Susumu Shirabe,[9] Ken Nagata,[10] Tetsuya Maeda,[10] Shigeo Murayama,[11] Yuishin Izumi,[1] Ryuji Kaji,[1] Masahito Yamada,[5] Hidehiro Mizusawa[6]

To cite: Fujita K, Harada M, Sasaki M, *et al*. Multicentre, multiobserver study of diffusion-weighted and fluid-attenuated inversion recovery MRI for the diagnosis of sporadic Creutzfeldt–Jakob disease: a reliability and agreement study. *BMJ Open* 2012;**2**: e000649. doi:10.1136/bmjopen-2011-000649

► Prepublication history for this paper is available online. To view this file please visit the journal online (http://bmjopen.bmj.com).

Received 21 November 2011
Accepted 20 December 2011

For numbered affiliations see end of article.

Correspondence to
Dr Masafumi Harada;
masafumi@clin.med.tokushima-u.ac.jp

ABSTRACT

Objectives: To assess the utility of the display standardisation of diffusion-weighted MRI (DWI) and to compare the effectiveness of DWI and fluid-attenuated inversion recovery (FLAIR) MRI for the diagnosis of sporadic Creutzfeldt–Jakob disease (sCJD).

Design: A reliability and agreement study.

Setting: Thirteen MRI observers comprising eight neurologists and five radiologists at two universities in Japan.

Participants: Data of 1.5-Tesla DWI and FLAIR were obtained from 29 patients with sCJD and 13 controls.

Outcome measures: Standardisation of DWI display was performed utilising b0 imaging. The observers participated in standardised DWI, variable DWI (the display adjustment was observer dependent) and FLAIR sessions. The observers independently assessed each MRI for CJD-related lesions, that is, hyperintensity in the cerebral cortex or striatum, using a continuous rating scale. Performance was evaluated by the area under the receiver operating characteristics curve (AUC).

Results: The mean AUC values were 0.84 (95% CI 0.81 to 0.87) for standardised DWI, 0.85 (95% CI 0.82 to 0.88) for variable DWI and 0.68 (95% CI 0.63 to 0.72) for FLAIR, demonstrating the superiority of DWI ($p<0.05$). There was a trend for higher intraclass correlations of standardised DWI (0.74, 95% CI 0.66 to 0.83) and variable DWI (0.72, 95% CI 0.62 to 0.81) than that of FLAIR (0.63, 95% CI 0.53 to 0.74), although the differences were not statistically significant.

Conclusions: Standardised DWI is as reliable as variable DWI, and the two DWI displays are superior to FLAIR for the diagnosis of sCJD. The authors propose that hyperintensity in the cerebral cortex or striatum on 1.5-Tesla DWI but not FLAIR can be a reliable diagnostic marker for sCJD.

ARTICLE SUMMARY

Article focus

- Evaluation of the reliability of diffusion-weighted imaging (DWI) display standardisation for the diagnosis of sporadic Creutzfeldt–Jakob disease (sCJD).
- Comparison between DWI and fluid-attenuated inversion recovery (FLAIR) for the diagnosis of sCJD.

Key messages

- Standardised DWI display is as reliable as observer-dependent DWI display.
- DWI is superior to FLAIR for the diagnosis of sCJD.
- Hyperintensity in the cerebral cortex or striatum on 1.5-Tesla DWI but not FLAIR can be a reliable diagnostic marker for sCJD.

Strengths and limitations of this study

- Strength of this study is the large number of physicians who participated in the observer performance study.
- This study was limited by the retrospective nature that may lead to a selection bias.

INTRODUCTION

Reliable detection of Creutzfeldt–Jakob disease (CJD) is imperative for infection control and treatment. MRI is useful for the early diagnosis of CJD,[1 2] whereas the utility of EEG and conventional cerebrospinal fluid (CSF) tests have been limited.[3] Diffusion-weighted imaging (DWI) and fluid-attenuated inversion recovery (FLAIR) are key techniques for the diagnosis of sporadic CJD (sCJD) with high sensitivity and specificity when assessed by expert neurologists or

neuroradiologists.[1 4 5] However, the utility of MRI for general neurologists or radiologists who are not familiar with diagnosing CJD remains elusive. Moreover, standardisation of MRI methodologies, which would be essential for the reproducible assessment of MRI findings of CJD cases, has not been achieved in previous studies.[1 4 5] DWI display conditions may particularly vary among institutions or operators,[6] which can give rise to inaccurate assessment of CJD-related lesions, specifically subtle abnormalities in the cerebral cortex. Meanwhile, although DWI seems superior to FLAIR for the detection of CJD lesions,[5] direct comparison of the two sequences is yet to be performed.

To address these issues, we investigated the utility of a newly proposed standardisation method of DWI display[6 7] and compared the effectiveness of DWI and FLAIR for the diagnosis of sCJD, particularly for differentiating between abnormal and normal signals by neurologists and radiologists who are not necessarily CJD experts. We conducted a multicentre, multiobserver case–control study and evaluated observer performance with receiver operating characteristics (ROC) analysis.

METHODS

Subjects

Patients diagnosed as having sCJD by the CJD Surveillance Committee of Japan[8] from October 2005 to September 2010 were eligible to participate in this study. The accuracy of the diagnosis was defined as follows: definite, that is, pathologically verified cases; probable, that is, cases with neuropsychiatric manifestations compatible with sCJD and periodic sharp wave complexes on EEG without pathological examinations and possible, that is, cases with the same findings as probable sCJD but no periodic sharp wave complexes on EEG.[8 9] WHO criteria[10] were not applied because the assay of CSF 14-3-3 protein, which is required by WHO criteria, was standardised only since April 2009 in Japan.[11] The prion protein gene (*PRNP*) was analysed in the open reading frame after extracting DNA from patients' blood.[12 13] For neuropathological examinations, brain sections were stained with routine techniques, and immunohistochemistry was performed using the mouse monoclonal antibody 3F4 (Senetek, MD Heights, Missouri, USA).[12] For PrP^{Sc} typing, frozen brain tissues were homogenised and analysed by western blot for proteinase K-resistant PrP using the 3F4 antibody.[14] Assays for CSF γ-isoform of 14-3-3 protein,[11] total τ protein (cut-off value, 1300 pg/ml)[15] and real-time quaking-induced conversion (RT-QUIC)[16] were performed in patients whose CSF samples were available. The following patients were eligible as disease controls: patients who were suspected to have prion disease by primary physicians but were denied to have prion disease by the Committee or those who were diagnosed as having other neurological disorders at Tokushima University Hospital and whose brain MRI showed no abnormal intensity in the cerebral cortex or striatum. We requested physicians who had referred patients to the Committee to provide initial MRI data of eligible patients.

This study was approved by the Medical Ethics Committee of Kanazawa University and the Ethics Committees of the Tokushima University Hospital and Tokyo Medical and Dental University. Written informed consent was obtained from all patients or their families.

Magnetic resonance imaging

DWI, b0 and FLAIR images were converted to the Digital Imaging and Communication in Medicine format. When the Digital Imaging and Communication in Medicine data contained patient information, it was excluded by one of the investigators (MH) before the observer performance study. All MRI studies were performed on 1.5-Tesla scanners at each hospital. Quadrature detection head coils or multichannel head coils were used. DWI was performed using the single-shot spin-echo echo planar imaging technique with the following parameters: repetition time, 4000–8000 ms; echo time, 70–100 ms; b value, 1000 s/mm^2; slice thickness, 5 mm; matrix size, 128×80 to 128×128; field of view, 220–230 mm and 16–20 contiguous axial sections parallel to a line through the anterior and posterior commissures were obtained from each patient. The scanning parameters of FLAIR were as follows: repetition time, 8000–10 000 ms; inversion time, 2000–2500 ms; effective echo time, 105–120 ms; matrix size, 256×192 to 320×224; field of view, 210–220 mm; slice thickness, 5–6 mm with 1–1.5 mm interslice gaps and 19–20 slices per patient.

Display methods

Two display methods were used for DWI: standardised and variable. In the standardised display, the window width and level settings were constant for all evaluations and could not be changed. Details of the standardised display have been reported elsewhere.[6] In brief, the window width and level were as follows: window width = SI_{b0} and window level = $SI_{b0}/2$, where SI_{b0} represents the signal intensity in the normal-appearing subcortical region on b0 imaging.[6] One radiologist (MH) manually measured SI_{b0} within a circular region of interest. The calculated window width and level were applied to all images. In the variable display mode, regarded as the most reliable for assessment of DWI, each observer was able to change the window width and level settings on the monitor according to preference. FLAIR was assessed with the variable display method because no standardised methods are currently available for FLAIR display.

Observer performance study

Eight neurologists (6–27 years of experience; mean, 12 years; board certified, six) and five radiologists (5–25 years of experience; mean, 12.8 years; board certified, four; neuroradiologist, one) participated in the observer performance study at The University of Tokushima Graduate School (persons, six; neurologists, three) and Tokyo Medical and Dental University

(persons, seven; neurologists, five including NS and YS). Before the test, the observers were informed that the purpose of the study was to evaluate their performance in detecting MRI lesions compatible with CJD, that is, hyperintensity in the cerebral cortex or striatum, regardless of signal changes in other regions including the thalamus. Three sessions were conducted: standardised DWI, variable DWI and FLAIR. To reduce the effect of learning, the interval between reading sessions was 1 week or longer. The order of the three sessions was randomised among the observers. Using computer randomisation, images of patients with and without sCJD were intermixed. All cases were presented in the same randomised order to the observers in each session. Each observer independently viewed all slices of each MRI study on the same type of monitors (Let'snote, Panasonic, Osaka, Japan) using INTAGE Realia Professional (Cubernet, Tokyo, Japan) run on Windows XP (Microsoft). The observers were allowed to adjust the window width and level only in variable DWI and FLAIR sessions but not in the standardised DWI session. Observers were blinded to any clinical information including age, sex and diagnosis.

Each observer used a continuous rating scale of a line-marking method to rate his or her confidence level on the paper format independently. At the left end of the line, a confidence level that lesions compatible with CJD were definitely absent was indicated, whereas at the right end, a confidence level that lesions were definitely present was indicated. Intermediate levels of confidence were indicated by the different positions on the line between the two ends. The distance between the left end and the marked point was converted to a confidence level that could range from 0 to 100, as described elsewhere.[17]

Statistical analyses

Observer performance was evaluated using ROC analysis with SPSS V.19 (IBM). The ROC curves for each observer indicated the ratio of the true-positive fraction to the false-positive fraction at each confidence level. The area under the ROC curve (AUC) was used to compare observer performance for accurately detecting CJD lesions. Intraclass correlations were calculated in the neurologist group, the radiologist group and for all observers by two-way random consistency measures using the SPSS software. In all the analyses, p values of <0.05 were considered statistically significant.

RESULTS

Patients and controls

MRI data from 85 patients were provided. Of these, 42 subjects from 15 hospitals (including authors' institutions) were eligible for this study after excluding cases that were diagnosed as having non-sporadic CJD or lacked the required MRI sequences. This study cohort included 29 patients with sCJD (men, 11; mean age, 71 years; duration before MRI, 4.4±6.1 months), three patients who were suspected of CJD but eventually diagnosed as negative by the Committee and 10 patients diagnosed as having other neurological disorders. Of the 29 sCJD patients, four had definite, 24 had probable and one had possible CJD. Twenty-six cases underwent *PRNP* analysis, 24 were homozygous for methionine at codon 129 and two were heterozygous with methionine and valine at codon 129. Of the four definite cases, PrP^{Sc} was type 1 in two cases, type 1+2 in one case and type 2 in one case. Eleven of 15 CSF samples from probable sCJD cases were positive for PrP^{Sc} by RT-QUIC (table 1).

Diagnoses for three prion-denied patients were immune-mediated encephalopathy, juvenile Alzheimer's disease and frontotemporal dementia. Other neurological controls were diagnosed with Alzheimer's disease, Parkinson's disease, spinocerebellar degeneration, vascular dementia, old cerebral infarction, benign paroxysmal positional vertigo, dizziness, temporal arteritis, cervical spondylosis and diabetic neuropathy.

Diagnostic performance

We investigated the diagnostic performance of standardised DWI, variable DWI and FLAIR images assessed by eight neurologists and five radiologists using ROC analysis. Mean AUC values obtained from the three sessions were compared within the neurologist group, the radiologist group and all observers (figure 1, table 2). The AUC values for standardised and variable DWI were not different within each professional group or for the total observer group. On the other hand, AUC values for FLAIR were significantly lower than DWI displayed by either method ($p<0.05$). Representative MRI scans are shown in figure 2.

Rating agreement

To measure the extent to which the observers agreed when rating the MRI findings, intraclass correlations were calculated. The intraclass correlations of the standardised DWI (0.74, 95% CI 0.66 to 0.83) and variable DWI (0.72. 95% CI 0.62 to 0.81) tend to be higher than that of FLAIR (0.63, 95% CI 0.53 to 0.74), specifically in the neurologist group, although the differences were not significant (figure 3).

DISCUSSION

We demonstrated that standardised DWI was as useful as variable DWI and that both DWI displays are superior to FLAIR for the diagnosis of sCJD when assessed by multiobservers with various specialty backgrounds.

Our standardisation method of DWI display was originally proposed as an easy-to-use way to decide the window width and level for DWI even in emergency settings.[6] Indeed, this method was demonstrated as useful for detecting acute ischaemic lesions on DWI.[7] Results of the present study show that the standardisation method is also reliable for diagnosis of sCJD, in which DWI is one of the key sequences. We suggest some advantages of standardised DWI over variable DWI, although there was no statistical difference between the two methods. First, standardised DWI can be helpful for

Table 1 Clinical profiles of patients with sporadic Creutzfeldt–Jakob disease

No	Age/sex	Diagnosis	Codon129/PrP^{Sc}	14-3-3/total τ	RT-QUIC	Pre-MRI duration (months)
1	69/M	Definite	MM/1	+/+	+	–2*
2	77/F	Definite	MM/1	+/+	+	19
3	75/F	Definite	ND/1+2	+/+	+	3
4	65/M	Definite	MM/2	–/–	–	12
5	69/M	Probable	MM	ND	–	0.5
6	72/F	Probable	MM	ND	ND	0.5
7	77/F	Probable	MM	–/–	+	0.5
8	72/M	Probable	MM	ND	ND	1
9	63/M	Probable	MM	+/+	+	1.5
10	88/F	Probable	MM	ND	ND	1.5
11	75/M	Probable	MV	ND	ND	1.5
12	56/M	Probable	MM	+/+	+	2
13	67/M	Probable	MM	+/+	–	2
14	70/M	Probable	MM	+/+	+	2
15	70/F	Probable	MM	+/+	+	2
16	74/F	Probable	MM	+/+	–	2
17	84/F	Probable	MM	+/–	+	2
18	85/F	Probable	MM	–/+	+	2
19	49/F	Probable	ND	+/+	+	2
20	74/F	Probable	MV	+/+	+	2.5
21	54/F	Probable	ND	ND	ND	2.5
22	61/M	Probable	MM	ND	ND	3
23	72/F	Probable	MM	+/–	–	3
24	81/F	Probable	MM	–/–	+	3
25	70/M	Probable	MM	+/+	+	6
26	83/F	Probable	MM	+/+	ND	9
27	67/F	Probable	MM	+/+	–	15
28	84/F	Probable	MM	+/+	–	26
29	57/F	Possible	MM	ND	ND	4

*MRI was obtained 2 months before the symptom onset.[2]
MM, homozygous for methionine; MV, heterozygous with methionine and valine; ND, not done; RT-QUIC, real-time quaking-induced conversion.

physicians who can refer only to hardcopies but not softcopies. Second, even for doctors who can readily refer to softcopies and thus variable DWI, the standardisation method can simplify assessment procedure without any disadvantages. Third, the standardisation can facilitate direct comparison of DWI findings from different CJD patients.

DWI and FLAIR have been reported as useful markers for the diagnosis of CJD. Of these, DWI has been assumed to be the most sensitive, although without direct evidence.[1 5 18] Hyperintensity in the cerebral cortices, the striatum or both indicates the diagnosis of CJD. The striatum hyperintensity is anterior dominant at early stages of the disease.[19] MRI lesion profiles reportedly differ among molecular subtypes of sCJD,[20 21] which was not reproduced in a recent study.[5] Zerr *et al*[4] proposed that high-signal abnormalities in caudate nucleus and putamen or at least two cortical regions (temporal, parietal or occipital lobes) either in DWI or FLAIR together with typical clinical signs can be diagnostic for probable sCJD. Based partly upon their report, 'high signal in caudate/putamen on MRI brain scan' has

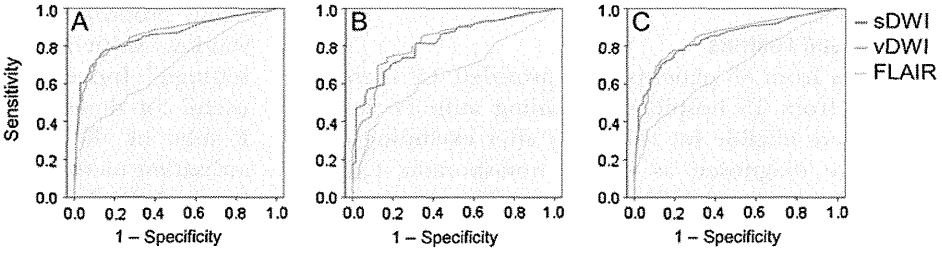

Figure 1 Receiver operating characteristic curves for each display in diagnosis of sporadic Creutzfeldt–Jakob disease. (A) Neurologists, (B) radiologists and (C) all observers. The true rate (sensitivity) is plotted as a function of the false-positive rate (1 – specificity). DWI, diffusion-weighted imaging; FLAIR, fluid-attenuated inversion recovery; sDWI, standardised DWI; vDWI, variable DWI.

Table 2 Areas under the receiver operating characteristic curves

	Neurologists	Radiologists	All observers
sDWI	0.86 (0.82 to 0.90)	0.82 (0.77 to 0.88)	0.84 (0.81 to 0.87)
vDWI	0.86 (0.82 to 0.90)	0.83 (0.77 to 0.89)	0.85 (0.82 to 0.88)
FLAIR	0.69 (0.63 to 0.75)	0.66 (0.58 to 0.73)	0.68 (0.63 to 0.72)

Means (95% CIs) are indicated.
DWI, diffusion-weighted imaging; FLAIR, fluid-attenuated inversion recovery; sDWI, standardised DWI; vDWI, variable DWI.

been used as one of the laboratory findings in the diagnostic criteria for probable sCJD in the European CJD Surveillance System (EUROCJD) since January 2010.[22] However, their criteria did not distinguish DWI and FLAIR, thereby maintaining ambiguity about the diagnostic values of MRI in situations where DWI is not available. Our data indicate that FLAIR without DWI is unreliable for the diagnosis of sCJD. On the other hand, high signals in the cerebral cortex have not been regarded as diagnostic in the EUROCJD criteria, probably because cortical abnormalities are less reliable on conventional MRI. Our results suggest that, using standardised or variable DWI but not FLAIR, cortical signals can also be used as a diagnostic marker.

Meanwhile, Young *et al*[23] reported that the sensitivity and the specificity of DWI and FLAIR for the diagnosis of CJD are 91% and 95%, respectively. More recently, Vitali *et al*[5] reported that hyperintensity greater on DWI than FLAIR is diagnostic for sCJD, whereas hyperintensity greater on FLAIR than DWI is characteristic for non-prion rapidly progressive dementia. Furthermore, reduction of apparent diffusion coefficient in subcortical (striatum) hyperintensity regions on DWI is supportive for sCJD.[5 24 25] These findings can be greatly helpful for differentiating sCJD from other rapidly progressive dementia. However, assessment of FLAIR lesions tends to vary among physicians, particularly among neurologists, as shown by the present study, and standardised methods for FLAIR or apparent diffusion coefficient map have not been established until date. Therefore, clinical criteria which require DWI but not necessarily FLAIR or apparent diffusion coefficient will be more readily applicable.

As many as 13 neurologists and radiologists from different institutions participated in the observer performance study, although the sample size of patients was relatively small. Notably, the observers had various specialty backgrounds such as stroke neurologists, neurophysiologists, experts in dementia or prion disease and general and neuroradiologists. This variety simulates practical situations in which the diagnosis of suspected CJD cases may be made by physicians who do not necessarily specialise in prion disease.

This study has some limitations. First, we did not evaluate patterns of cortical involvement suggestive of sCJD[4 5] because we had to address whether DWI or FLAIR is suitable for detecting cortical lesions in the first place. Second, we did not assess the difference among sCJD subtypes[21] because majority of our cases had a typical phenotype and were homozygous for methionine; thus, they were compatible with MM1 sCJD. Until date, MM2 thalamic-type sCJD remains a diagnostic challenge in MRI-based assessment; thalamic hypoperfusion or hypometabolism on SPECT or PET can be useful.[26] Third, majority of the control patients were not those who were suspected to have CJD. However, the

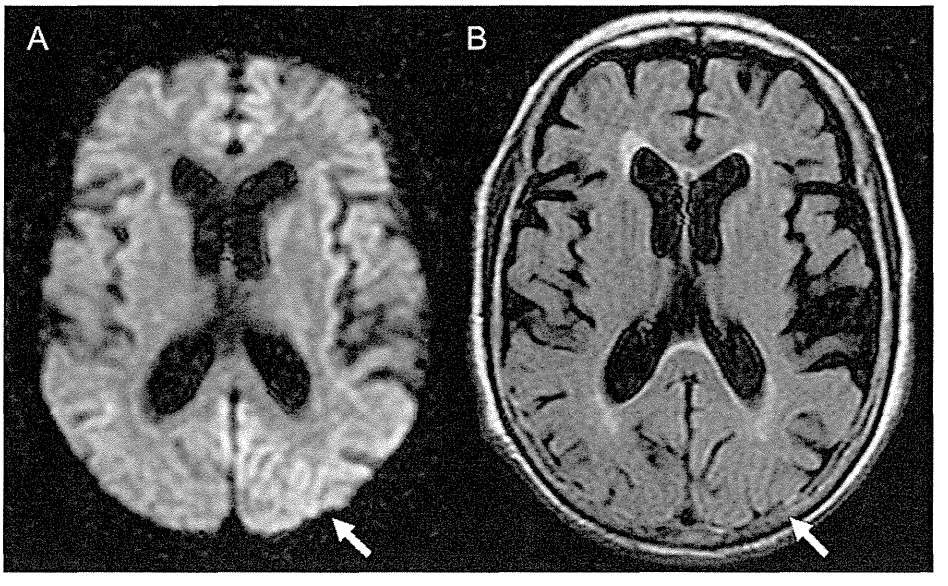

Figure 2 Representative MRI of a sporadic Creutzfeldt–Jakob disease patient (case 17). Abnormal hyperintensity in the cerebral cortex is evident on standardised diffusion-weighted imaging (A, arrow) but obscure on fluid-attenuated inversion recovery (B, arrow).

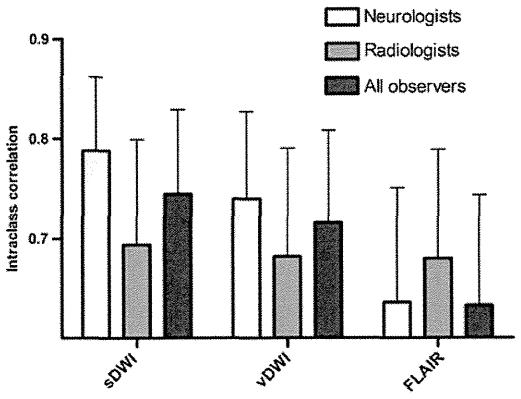

Figure 3 Intraclass correlations for each display. Error bars represent upper limits of 95% CIs. DWI, diffusion-weighted imaging; FLAIR, fluid-attenuated inversion recovery; sDWI, standardised DWI; vDWI, variable DWI.

principle aim of the present study was to establish a display method, which reliably distinguishes potentially CJD-associated signals from normal signals. Thus, our results provide a practical foundation for utilising DWI as a general diagnostic marker of sCJD when combined with previous findings.[1 4 5]

Although neuropathological confirmation of the diagnosis of sCJD was obtained in few cases, we performed RT-QUIC, a newly established CSF PrP^{Sc} amplification assay which achieved >80% sensitivity and 100% specificity for CJD.[16] Overall, 15 of 29 cases (51.7%) were pathologically proven or confirmed by RT-QUIC to have CJD. There were no significant differences in MRI findings between sCJD patients with and without positive results of CSF 14-3-3 protein, total τ protein or RT-QUIC. It will be important to further evaluate accurate diagnostic ability (sensitivity and specificity) of DWI in a prospective cohort of suspected CJD patients, that is, consecutive patients registered to the CJD surveillance who will also undergo CSF confirmation tests or neuropathological analyses.

In conclusion, we suggest that hyperintensity in the cerebral cortex or striatum assessed on the standardised or variable DWI scanned with 1.5-Tesla machines can be a reliable first-line on-site diagnostic marker for sCJD.

Author affiliations
[1]Department of Clinical Neuroscience, Institute of Health Biosciences, The University of Tokushima Graduate School, Tokushima, Japan
[2]Department of Radiology, Institute of Health Biosciences, The University of Tokushima Graduate School, Tokushima, Japan
[3]Advanced Medical Science Center, Iwate Medical University, Morioka, Japan
[4]Department of Neurology, Kamagaya-Chiba Medical Center for Intractable Neurological Disease, Kamagaya General Hospital, Kamagaya, Japan
[5]Department of Neurology and Neurobiology of Aging, Kanazawa University Graduate School of Medical Science, Kanazawa, Japan
[6]Department of Neurology and Neurological Science, Graduate School, Tokyo Medical and Dental University, Tokyo, Japan
[7]Department of Neurology, Aoba Neurosurgical Clinic, Sendai, Japan
[8]Department of Molecular Microbiology and Immunology, Nagasaki University Graduate School of Biomedical Sciences, Nagasaki, Japan
[9]Center for Health and Community Medicine, Nagasaki University, Nagasaki, Japan
[10]Department of Neurology, Research Institute for Brain and Blood Vessels, Akita, Japan
[11]Department of Neuropathology (Brain Bank for Aging Research), Tokyo Metropolitan Institute of Gerontology, Tokyo, Japan

Acknowledgements We thank Tetsuyuki Kitamoto (Tohoku University Graduate School of Medicine) for *PRNP* analysis, western blotting of PrP and neuropathological investigations; Yuka Terasawa, Yoshimitsu Shimatani, Ai Miyashiro (Department of Clinical Neuroscience, The University of Tokushima Graduate School), Hideki Otsuka, Naomi Morita, Yoichi Otomi (Department of Radiology, The University of Tokushima Graduate School), Satoru Ishibashi, Takumi Hori, Akira Machida (Department of Neurology and Neurological Science, Tokyo Medical and Dental University), Isamu Ohashi and Takashi Katayama (Department of Radiology, Tokyo Medical and Dental University) for participation in the observer performance study. We also thank Joe Senda (Nagoya University), Yuko Nemoto (Chiba Medical Center), Akio Kawakami (Kaetsu Hospital), Isao Sasaki (Mizunomiyako Memorial Hospital), Shigeyuki Kojima (Matsudo Municipal Hospital), Motohiro Yukitake (Saga University), Hiroyuki Murai (Iizuka Hospital), Hideki Mizuno (Kohnan Hospital), Akira Arai (Aomori Prefectural Central Hospital), Masamitsu Yaguchi (Shinoda General Hospital), Takanori Oikawa (South Miyagi Medical Center) and all other collaborative physicians for providing MRI data of the patients. We thank the members of the CJD Surveillance Committee of Japan for their support of this work.

Funding This study was supported by Grants-in-Aid from the Research Committee of Surveillance and Infection Control of Prion Disease and from the Research Committee of Prion Disease and Slow Virus Infection, the Ministry of Health, Labour and Welfare of Japan.

Competing interests None.

Patient consent Obtained.

Ethics approval This study was approved by the Medical Ethics Committee of Kanazawa University and the Ethics Committees of the Tokushima University Hospital and Tokyo Medical and Dental University.

Contributors KF, MH, MS, TY, KSak, TH, NS, YS, KSat, SS, MY and HM: design/conceptualisation of the study. MH, KSak, TH, NS, YS, KSat, RA, KN, TM, SM and YI: acquisition of data. KF, MH, MS, RA, RK, MY and HM: analysis/interpretation of the data. MH: statistical analyses. KF, MH, MS, TY, KSak, TH, NS, YS, KSat, RA, SS, KN, TM, SM, YI, RK, MY and HM: drafting/revising the manuscript. All authors contributed to final approval of the version to be published.

Provenance and peer review Not commissioned; externally peer reviewed.

Data sharing statement There are no additional data available.

REFERENCES

1. Shiga Y, Miyazawa K, Sato S, *et al.* Diffusion-weighted MRI abnormalities as an early diagnostic marker for Creutzfeldt–Jakob disease. *Neurology* 2004;63:443–9.
2. Satoh K, Nakaoke R, Nishiura Y, *et al.* Early detection of sporadic CJD by diffusion-weighted MRI before the onset of symptoms. *J Neurol Neurosurg Psychiatry* 2011;82:942–3.
3. Chitravas N, Jung RS, Kofskey DM, *et al.* Treatable neurological disorders misdiagnosed as Creutzfeldt–Jakob disease. *Ann Neurol* 2011;70:437–44.
4. Zerr I, Kallenberg K, Summers DM, *et al.* Updated clinical diagnostic criteria for sporadic Creutzfeldt–Jakob disease. *Brain* 2009;132:2659–68.
5. Vitali P, Maccagnano E, Caverzasi E, *et al.* Diffusion-weighted MRI hyperintensity patterns differentiate CJD from other rapid dementias. *Neurology* 2011;76:1711–19.
6. Sasaki M, Ida M, Yamada K, *et al.* Standardizing display conditions of diffusion-weighted images by using concurrent b0 images: a multivendor multi-institutional study. *Magn Reson Med Sci* 2007;6:133–7.
7. Hirai T, Sasaki M, Meada M, *et al*; Acute Stroke Imaging Standardization Group-Japan (ASIST-Japan). Diffusion-weighted imaging in ischemic stroke: effect of display method on observers' diagnostic performance. *Acad Radiol* 2009;16:305–12.
8. Nozaki I, Hamaguchi T, Sanjo N, *et al.* Prospective 10-year surveillance of human prion diseases in Japan. *Brain* 2010;133:3043–57.
9. Masters CL, Harris JO, Gajdusek DC, *et al.* Creutzfeldt–Jakob disease: patterns of worldwide occurrence and the significance of familial and sporadic clustering. *Ann Neurol* 1979;5:177–88.